Cell-Mediated, Oxidatively Degradable Polyurethane/Ceramic Tissue Scaffolds for Bone and Articular Joint Repair

By

Dustin Mitchell Groff

Thesis

Submitted to the Faculty of the

Graduate School of Vanderbilt University

in partial fulfillment of the requirements

for the degree of

MASTER OF SCIENCE

in

Chemical Engineering

August 9, 2019

Nashville, Tennessee

Approved:

Scott A. Guelcher, Ph.D

Jamey D. Young, Ph.D.

DEDICATIONS

Dedicated to my wife, Veronica Groff, who has supported me throughout this process and always been encouraging of my dream

To my family and friends who have always believed in me and taught me how to succeed

ACKNOWLEGMENTS

I would first like to thank my thesis advisor, Dr. Scott Guelcher, for all his guidance and support throughout my tenure at Vanderbilt University. I am thankful for all the opportunities he afforded me to learn and grow as a research scientist, including collaboration with many labs at Vanderbilt and industry leaders in the medical device field. These skills are invaluable and will serve me well for the rest of my career. I would also like to thank the many collaborators that have supported my effort including the Vanderbilt Center for Bone Biology and others within the Biomedical Engineering Department such as Dr. Mukesh Gupta, Dr. Craig Duvall and Prarthana Patil. A special thanks to the Julie Sterling Lab including Alyssa Merkel and Josh Johnson, and also to Sasi Uppuganti in the Jeff Nyman lab for all his help.

I would like to extend a special thanks to all the lab members of Dr. Scott Guelcher Bone Tissue Engineering lab for all their support and guidance in my studies. The Guelcher lab manager, Katarzyna (Kasia) Zienkiewicz, was invaluable in my efforts in the lab. I would like to thank you for your patience and expertise in your mentorship in wet lab chemistry. Thank you to Dr. Madison McGough, Dr. Sichang Lu, Dr. Joseph Vanderburgh, Thomas Spoonmore, Greg Lowen, Lauren Boller, and David Florian for all your help in lab and friendship. You have all made my time at Vanderbilt memorable and fun. I would also like to acknowledge the undergraduate students who have helped me achieve my research goals including Cody Dykes, Mollie Maples, Monica Guadarrama, and Anahí Mejia-Contreras.

TABLE OF CONTENTS

Page

LIST OF TABLES

Table Caption Page

LIST OF FIGURES

NOMENCLATURE

AG	Autograft	PBS	Phosphate-buffered saline
HA	Hydroxyapatite	SDS	Sodium dodecyl sulfate
CaP	Calcium Phosphate	DB	Dual barrel
PMMA	Poly(methyl methacrylate)	TBME	Tert-butyl-methyl ether
PUR	Polyurethane	GC-MS	gas chromatography-mass spectrometry
LTI	Lysine-triisocyanate	NS	Nanostim^{TM} Synthetic Bone Paste
PEUR	Poly(ester urethane)	TGA	Thermogravimetric analysis
PTKUR	Poly(thioketal urethane)	XRD	X-ray diffraction
ROS	Reactive oxygen species	AOI	Area of interest
nHA	Nanocrystalline hydroxyapatite	VOI	Volume of Interest
FDM	Fused deposition modeling	BVF	Bone void filler
TPKTUR	Thermoplastic poly(thioketal urethane)	AM	Additive manufacturing
PCL	Polycaprolactone	PLA	Polylactide
TK	Thioketal	TPUR	Thermoplastic polyurethane
^{1}H NMR	Hydrogen nuclear magnetic resonances	MEE	2-mercaptoethyl ether
DMSO	Dimethyl sulfoxide	HDI	Hexane diisocyanate
DMP	2,2-dimethoxypropane	PTSA	P-toluenesulphonic acid monohydrate
FeAA	Iron (III) acetylacetone	EDDT	2,2′-(ethylenedioxy) diethanethiol
XPS	X-ray photoelectron spectroscopy	THF	Tetrahydrofuran

hMSCs	Human mesenchymal stem cells	AFM	Atomic force microscopy
DMF	Dimethyl formamide	SAXS	Small angle x-ray diffraction
DBTDL	Dibutylin dilaurate	DSC	Differential scanning spectrometry
GPC	Gel permeation chromatography	WAXS	Wide angle x-ray diffraction
BDO	Butane diol	DMA	Dynamic mechanical analysis
FTIR	Fourier-transformed infrared spectrometry		

CHAPTER 1

INTRODUCTION

Bone tissue grafts are scaffolding constructs necessary for the treatment and healing of many forms of bone disease and fractures, especially when the defect or dissection is greater than the critical size to heal naturally.[1] Currently, Autograft (AG) bone is the gold standard for critically sized bone defects as tissue for the patient's own body by nature is highly osteoinductive and promotes osteogenesis without the risks of immune rejection.[2, 3] Bone graft procedures in the United States occur approximately 1.6 million times annually, but for many of these procedures AG is not a suitable option as the supply is often limited, and these procedures can lead to donor site morbidity, infection and pain for the patient.[4] Mineralized allografts have immerged as a substitute to AG, but represent a high risk of infection and immune rejection.[5, 6] Bioengineered synthetic bone tissue grafts present a unique solution for artificial bone grafts. The ideal bone graft biomaterial will enable bone tissue regeneration by promoting cellular activity, osteogenesis and will degrade to non-toxic byproducts at rates aligning with tissue infiltration. For purpose of weight-bearing bone tissue biomaterials with high strength capable of maintaining structural integrity while remodeling are particularly critical.[7, 8]

There are many biomaterials on the market aimed at solving this problem. Poly(methyl methacrylate) (PMMA) is a biocompatible bone graft with high strength and ideal mechanical properties for weight bearing sites, but the graft is non-resorbable and will remain in the patient for the remainder of life. These bone grafts are highly susceptible to infection which requires long-term systemic antibiotics and multiple surgeries for repair.[6] Ceramic materials have also been

extensively used as a synthetic alternative to AG as many ceramic materials, such as calcium phosphate (CaP) and hydroxyapatite (HA), mimic the natural chemical composition of bone.[8] Both HA and CaP have been shown to elicit an osteoconductive response and promote osteoblast differentiation and mineralization.[9] These ceramic materials generally have favorable mechanical properties allowing their use in weight-bearing sites but, due to their brittle nature, generally are not used at weight-bearing sites as they pose a significant risk of mechanical failure and reinjury.[8]

Polyurethanes (PURs) bone grafts have been used by the Guelcher lab and others as a suitable solution.[10-17] PURs are derived of two liquid reactants that when mixed rapidly set and form a stable polymeric matrix. The advantages of PURs include tunable mechanical properties, a flexible range of application, biocompatibility and degradation to non-toxic byproducts. The Guelcher lab has previously investigated lysine-triisocyanate (LTI)-derived PURs with polyester triols to create a poly(ester urethane) (PEUR) bone grafts.[17-19] These scaffolds showed promising results, but the grafts degraded via a hydrolytic mechanism.[18, 20] This led to rapid clearance of the bone graft, well before the establishment of new bone formation. To resolve this issue our lab and others have developed a biodegradable poly(thioketal urethane) (PTKUR) which is stable in hydrolytic environments and which will instead degrade in the presence of reactive oxygen species (ROS) typically present at the site of bone graft procedures.[21, 22]

1.1 Chapter Overview

The primary goal of this thesis was to create a bone graft, leveraging many of these technologies, capable of translation to pre-clinical trial for an eventual 510(k) FDA submission.

Chapter 2: ***Develop a polymer-ceramic bone graft capable of translation to a manufacturing environment which degrades via an oxidative pathway and invokes an osteogenic response***

Our group has previously investigated nanocrystalline hydroxyapatite (nHA) (<200nm) which due to increased surface area has been shown to increase the osteogenic response.[9, 16] We have shown this effect is amplified by grafting LTI to surface hydroxyl groups present on nHA before eventual formation of PURs. By grafting nHA into the polymeric framework, the ceramic material is evenly mixed throughout the bone graft as opposed to an nHA/PUR blend composite.[16, 23] PTKURs have previously been shown to selectively degrade in the presence of ROS secreted by cells.[21, 22] We believe that by combining nHA-LTI grafted solution (referred to as prepolymer) with the a cell-degradable poly(thioketal), optimal synthetic bone graft properties can be achieved. This work will investigate the feasibility of translating nHA-PKTUR composite to a manufacturing settings by assessing polymer purity, long-term stability, packaging configurations and overall product specification performances. These data are all necessary for an eventual FDA submission and a pathway to clinical trials.

Chapter 3: ***Test the nHA-LTI-PTKUR formulation in an* in vivo *rabbit femoral condyle defect to assess cellular infiltration, response and graft degradation***

Our group has previously shown that hydrolytically degradable PEURs resorb too quickly *in vivo* eliciting a highly fibrotic response and discouraging natural bone healing.[20, 24] We looked to correct this by implementing the nHA-LTI-PTKURs *in vivo* to slow down resorption of the polymeric scaffold. This chemistry allowed for a cell-mediated degradation, with the goal of degrading polymer scaffold at rates aligned with bone tissue infiltration.[21] Prior work revealed the nHA-LTI-PTKURs *in vivo* were stable and biocompatible but failed to degrade quickly or at a

relevant biological rate.[22] To resolve this issue, we proposed a long-term 18-month rabbit study looking at nHA-LTI-PTKURs with varying porosity and additives to allow for greater cellular infiltration to increase the rate of bone graft degradation. This study revealed increased cellular infiltration and greater bone remodeling, but interestingly by both an intramembranous ossification and unexpectedly an endochondral ossification.

Chapter 4: ***Develop a thermoplastic elastomeric alternative PUR which degrades in the presence of ROS capable of Fuse Deposition Manufacturing (FDM) 3D Printing***

Thermoplastic polymers are essential components of many biomedical devices and implants.[25-27] They are particularly useful for fused deposition modeling (FDM), a 3D printing technique utilizing thermoset elastomers melted above their T_m and extruded layer by layer.[28] Currently, polyesters are the most common bioresorbable polymer available for printing, yet these polymers are susceptible to an auto-catalytic degradation in which acidic break-down byproducts accelerate the degradation, leading to an imbalance between the rate of tissue formation and scaffold degradation.[22, 28, 29] PTKURs have emerged as a novel chemistry for the creation of hydrolytically stable polymers which degrade by a first-order oxidative mechanism, allowing for cell infiltration to dictate scaffold degradation kinetics.[30] In this work, we created a novel thermoplastic poly(thioketal urethane) (TPTKUR) elastomer with a tunable, cell-mediated degradation mechanism as an alternative thermoplastic for additive manufacturing techniques. The long-term objective is to fabricate TPTKUR biomedical implants with the desired mechanical and morphometric properties to improve wound healing by aligning the rate of tissue infiltration with scaffold degradation.

1.2 References

1. Schmidt-Bleek, K.; Kwee, B. J.; Mooney, D. J.; Duda, G. N., Boon and Bane of Inflammation in Bone Tissue Regeneration and Its Link with Angiogenesis. *Tissue Eng Part B Rev* **2015,** *21* (4), 354-64.
2. Albrektsson, T.; Johansson, C., Osteoinduction, osteoconduction and osseointegration. *Eur Spine J* **2001,** *10 Suppl 2*, S96-101.
3. Giannoudis, P. V.; Dinopoulos, H.; Tsiridis, E., Bone substitutes: an update. *Injury* **2005,** *36 Suppl 3*, S20-7.
4. Hollinger, J. O.; Kleinschmidt, J. C., The critical size defect as an experimental model to test bone repair materials. *J Craniofac Surg* **1990,** *1* (1), 60-8.
5. Beaman, F. D.; Bancroft, L. W.; Peterson, J. J.; Kransdorf, M. J., Bone graft materials and synthetic substitutes. *Radiologic Clinics* **2006,** *44* (3), 451-461.
6. Younger, E. M.; Chapman, M. W., Morbidity at bone graft donor sites. *J Orthop Trauma* **1989,** *3* (3), 192-195.
7. Bohner, M., Design of ceramic-based cements and putties for bone graft substitution. *Eur Cell Mater* **2010,** *20*, 1-12.
8. Wagoner Johnson, A. J.; Herschler, B. A., A review of the mechanical behavior of CaP and CaP/polymer composites for applications in bone replacement and repair. *Acta Biomaterialia* **2011,** *7* (1), 16-30.
9. Webster, T. J.; Ergun, C.; Doremus, R. H.; Siegel, R. W.; Bizios, R., Enhanced functions of osteoblasts on nanophase ceramics. *Biomaterials* **2000,** *21* (17), 1803-1810.
10. Adhikari, R.; Gunatillake, P. A.; Griffiths, I.; Tatai, L.; Wickramaratna, M.; Houshyar, S.; Moore, T.; Mayadunne, R. T.; Field, J.; McGee, M.; Carbon, T., Biodegradable injectable polyurethanes: synthesis and evaluation for orthopaedic applications. *Biomaterials* **2008,** *29* (28), 3762-3770.
11. Adolph, E. J.; Guo, R.; Pollins, A. C.; Zienkiewicz, K.; Cardwell, N.; Davidson, J. M.; Guelcher, S. A.; Nanney, L. B., Injected biodegradable polyurethane scaffolds support tissue infiltration and delay wound contraction in a porcine excisional model. *Journal of Biomedical Materials Research Part B: Applied Biomaterials* **2015**.
12. Dumas, J. E.; Davis, T.; Holt, G. E.; Yoshii, T.; Perrien, D. S.; Nyman, J. S.; Boyce, T.; Guelcher, S. A., Synthesis, characterization, and remodeling of weight-bearing allograft bone/polyurethane composites in the rabbit. *Acta Biomaterialia* **2010,** *6* (7), 2394-2406.
13. Fernando, S.; McEnery, M.; Guelcher, S., Polyurethanes for bone tissue engineering. *Advances in Polyurethane Biomaterials* **2016**, 481.
14. Guelcher, S. A.; Patel, V.; Gallagher, K. M.; Connolly, S.; Didier, J. E.; Doctor, J. S.; Hollinger, J. O., Synthesis and In Vitro Biocompatibility of Injectable Polyurethane Foam Scaffolds. *Tissue Engineering* **2006,** *12* (5), 1247-59.
15. Guelcher, S. A.; Srinivasan, A.; Dumas, J. E.; Didier, J. E.; McBride, S.; Hollinger, J. O., Synthesis, mechanical properties, biocompatibility, and biodegradation of polyurethane networks from lysine polyisocyanates. *Biomaterials* **2008,** *29* (12), 1762-1775.
16. Lu, S.; McGough, M.; Rogers, B.; Wenke, J.; Shimko, D.; Guelcher, S., Resorbable nanocomposites with bone-like strength and enhanced cellular activity. *Journal of Materials Chemistry B* **2017,** *5* (22), 4198-4206.
17. Lu, S.; McGough, M. A.; Shiels, S. M.; Zienkiewicz, K. J.; Merkel, A. R.; Vanderburgh, J. P.; Nyman, J. S.; Sterling, J. A.; Tennent, D. J.; Wenke, J. C., Settable polymer/ceramic

composite bone grafts stabilize weight-bearing tibial plateau slot defects and integrate with host bone in an ovine model. *Biomaterials* **2018**.
18. Hafeman, A. E.; Zienkiewicz, K. J.; Zachman, A. L.; Sung, H.-J.; Nanney, L. B.; Davidson, J. M.; Guelcher, S. A., Characterization of the degradation mechanisms of lysine-derived aliphatic poly (ester urethane) scaffolds. *Biomaterials* **2011,** *32* (2), 419-429.
19. Nagata, M.; Oi, A.; Sakai, W.; Tsutsumi, N., Synthesis and properties of biodegradable network poly (ether-urethane) s from L-lysine triisocyanate and poly (alkylene glycol) s. *Journal of Applied Polymer Science* **2012,** *126* (S2).
20. Dumas, J. E.; Prieto, E. M.; Zienkiewicz, K. J.; Guda, T.; Wenke, J. C.; Bible, J.; Holt, G. E.; Guelcher, S. A., Balancing the Rates of New Bone Formation and Polymer Degradation Enhances Healing of Weight-Bearing Allograft/Polyurethane Composites in Rabbit Femoral Defects. *Tissue Engineering Part A* **2014,** *20* (1-2), 115-129.
21. Martin, J. R.; Gupta, M. K.; Page, J. M.; Yu, F.; Davidson, J. M.; Guelcher, S. A.; Duvall, C. L., A porous tissue engineering scaffold selectively degraded by cell-generated reactive oxygen species. *Biomaterials* **2014,** *35* (12), 3766-3776.
22. McEnery, M. A.; Lu, S.; Gupta, M. K.; Zienkiewicz, K. J.; Wenke, J. C.; Kalpakci, K. N.; Shimko, D. A.; Duvall, C. L.; Guelcher, S. A., Oxidatively degradable poly (thioketal urethane)/ceramic composite bone cements with bone-like strength. *RSC advances* **2016,** *6* (111), 109414-109424.
23. Liu, Q.; de Wijn, J. R.; de Groot, K.; van Blitterswijk, C. A., Surface modification of nano-apatite by grafting organic polymer. *Biomaterials* **1998,** *19* (11), 1067-1072.
24. Hafeman, A. E.; Zienkiewicz, K. J.; Zachman, A. L.; Sung, H.-J.; Nanney, L. B.; Davidson, J. M.; Guelcher, S. A., Characterization of the degradation mechanisms of lysine-derived aliphatic poly(ester urethane) scaffolds. *Biomaterials* **2011,** *32* (2), 419-429.
25. Spaans, C. J.; De Groot, J. H.; Belgraver, V. W.; Pennings, A. J., A new biomedical polyurethane with a high modulus based on 1,4-butanediisocyanate and e-caprolactone. *Journal of Materials Science: Materials in Medicine* **1998,** *9*, 675-678.
26. Spaans, C. J.; De Groot, J. H.; Van der Molen, L. M.; Pennings, A. J., New biodegradable polyurethane-ureas, polyurethane and polyurethane-amide for in-vivo tissue engineering: structure-properties relationships. *Polymeric Materials Science and Engineering* **2001,** *85*, 61-62.
27. Yilgor, I.; Yilgor, E.; Wilkes, G., Critical parameters in designing segmented polyurethanes and their effect on morphology and properties: A comprehensive review. *Polymer* **2015,** *58*, A1-36.
28. Chia, H. N.; Wu, B. M., Recent advances in 3D printing of biomaterials. *Journal of Biological Engineering* **2015,** *9* (1), 4.
29. Feuerbach, T.; Callau-Mendoza, S.; Thommes, M., Development of filaments for fused deposition modeling 3D printing with medical grade poly(lactic-co-glycolic acid) copolymers. *Pharm Dev Technol* **2018**, 1-7.
30. Martin, J. R.; Gupta, M. K.; Page, J. M.; Yu, F.; Davidson, J. M.; Guelcher, S. A.; Duvall, C. L., A porous tissue engineering scaffold selectively degraded by cell-generated reactive oxygen species. *Biomaterials* **2014,** *35* (12), 3766-76.

CHAPTER 2

DEVELOPMENT OF MANUFACTURABLE nHA-LTI-PTKURs WITH HIGH PURITY, STABLITY AND CAPABLE OF AN OSETEOCONDUTIVE RESPONSE

2.1 Abstract

Bone cements are commonly used in orthopedic operations as a bone void filler to enable recovery and bone formation following disease or trauma. There are currently cements capable of filling high load/weight bearing bone sites, yet these fillers lack the ability to degrade over time. Ceramic bone cements are also available for use and are highly biocompatible and osteoinductive yet are not capable of withstanding high loads. Our group has developed a PUR cement capable of withstanding forces exceeding that of trabecular bone and which degrades at a rate equivalent to that of cell infiltration by crosslinking a new poly(thioketal) (PTK) diol with lysine triisocyanate (LTI) grafted to nanocrystalline hydroxyapatite (nHA). In this work, we examine the capacity for translation to a manufacturing setting and eventual FDA submission.

2.2 Introduction

Injectable, degradable and settable bone cements with bone-like strength are highly sought after for restoring function to damaged or fractured bone, especially at weight bearing sites near intra-articular joints. Synthetic bone grafts with high load capacities are advantageous as host tissue is not required for repairing damaged bone, allowing for less-invasive orthopedic surgeries and faster patient recovery.[1] Currently, synthetic bone cements with high load strength, such as poly(methyl methacrylate) (PMMA), are available for use, but these grafts are non-resorbable. This can lead to graft rejection or infections, which lead to serious complications and typically

multiple surgeries.[2-4] Ceramic bone grafts, such as hydroxyapatite (HA) and tricalcium phosphates (TCP), are considered osteoinductive and highly biocompatible.[5-7] These ceramic grafts will integrate and resorb with host bone, but they are stiff and brittle, and are currently only cleared by the FDA as bone void fillers (BVF).[5, 8, 9] The limitation of mechanical properties precludes their use in locations considered critical to the stability of the skeletal system.[5] There remains a need for mechanically stable bone cement that will readily resorb into the host tissue at a biologically relevant rate, equal to that of cell infiltration into the scaffold. To meet these requirements, our lab has developed a novel composite scaffold which incorporates synthetic ceramics and resorbable urethane-based polymers to integrate the osteoinductive properties of the ceramic into the mechanically stable and biocompatible framework of a PUR.

Polyurethanes (PURs) have been extensively studied in the Guelcher group and others as a solution to a wide range of tissue engineering problems.[10-14] PURs consist of two liquid phases which, when combined in specific ratios, rapidly form an extensively crosslinked polymer network with tunable mechanical properties for a variety of applications. The Guelcher lab has worked primarily with lysine triisocyanate (LTI) as the isocyanate-phase and either polycaprolactones (PCLs) or polyester as the polyol-phase for the creation of PURs bone grafts.[15-19] While these grafts have shown success in bone void filler applications, in order to increase mechanical properties and induce an osteogenic and osteoconductive response, ceramics such as HA or TCP have been incorporated into the polymeric scaffolding. Nanocrystalline hydroxyapatite (nHA) particles (<200 nm) are believed to achieve even greater osteoconductive properties due to increased surface area exposure to the bone microenvironment.[20, 21] A previous study has shown that the surface hydroxyl (OH) groups present on the surface of nHA particles can be used to graft to the primary NCO group on LTI (nHA-LTI prepolymer) to greatly increase the dispersion of the

ceramic within the polymeric framework.[20] This nHA incorporation into the bone graft increases both mechanical properties and the osteogenic response *in vitro.*[20, 22]

Poly(ester urethanes) (PEURs) have been extensively utilized in the Guelcher group as a degradable, biocompatible bone graft, but these polymers have been shown to rapidly degrade *in vivo* and create regions of fibrotic tissue responses, especially in weight bearing models.[14, 18, 22] PEURs undergo an autocatalytic hydrolysis *in vivo* which is believed to be responsible for the rapid clearance of polymer, without allowing establishment of the natural tissue response for bone remodeling. To alleviate this problem, a short chain thioketal (TK) diol was selected as a hydrolytically stable polyol, which degrades in the presence of reactive oxygen species (ROS) commonly present at the site of implantation.[23-25] The hydrolytically stable poly(thioketal urethanes) (PTKURs) allows the degradation rate of the bone graft to be dictated by the rate of cellular infiltration into the scaffold.[23, 24] The cell-mediated degradation mechanism combined with the nHA-LTI grafted prepolymer are a promising solution for weight-bearing applications and have shown success in preliminary studies.

While this new composite has shown great promise in early models, there remain unanswered questions pivotal to the successful scaleup and transfer of this technology to a clinical setting. The aims of this paper are to answer questions necessary for the transition of this product from a lab setting to manufacturing, include the grafting kinetics of the nHA-LTI prepolymer and its overall stability, the purity and scaleup of the short chain TK diol, the long-term packaging, and cytotoxicity of the product. This work will lead to preclinical trials and eventually FDA submission, moving this product through the pathways necessary for release for use in patients.

2.3 Materials and Methods

Materials. All reagents necessary for TK diol synthesis including thioglycolic acid, 2,2-dimethoxypropane, bismuth chloride, lithium aluminum hydride, and various solvents (tetrahydrofuran, acetonitrile) were obtained from Sigma (St. Louis, MO). Crude lysine triisocyanate was purchased from Jinana Haohua Industry Co., LTD (Jinana, China) and treated in house by two serial carbon treatments in tert-methyl-butyl ether for 24 hours at 70 ºC to remove oligomers and various impurities. Nanocrystalline hydroxyapatite (nHA) was purchased from Sigma and dried at 80 ºC under vacuum for a minimum of 24 hours before use.

TK Diol Synthesis. The reaction catalyst, bismuth (III) chloride, was added to a dry 3-neck flask that was dried under vacuum using a hot air gun for approximately 5 minutes to ensure completely dry conditions. The vessel was purged with nitrogen and maintained at positive pressure. Acetonitrile, thioglycolic acid and 2,2-dimethoxypropane were sequentially added to the flask and reacted at room temperature for 24 hours. The intermediate carboxyl-end functionalized product was then filtered with a Buchner funnel and isolated from solvent by rotary evaporation at 35 ºC (Buchi Rotovap R-200). The intermediate product was then dried overnight under vacuum to ensure complete removal of residual solvents. The dried intermediate was dissolved in tetrahydrofuran (THF). A 3-neck flask was prepared for reduction by adding a condenser at 15 ºC capped with a one-way glass stopcock, an addition funnel, and a rubber stopcock. The vessel was dried under vacuum, purged with dry nitrogen, and kept under positive pressure. Lithium aluminum hydride ($LiAlH_4$) was added to the reactor and dissolved in diethyl ether. The reactor was resealed and placed into an ice bath. The carboxyl terminated intermediate was charged into the addition funnel and added to the $LiAlH_4$ solution dropwise. After all the TK intermediate was added to the reaction, the ice bath was replaced with an oil bath and the solution refluxed at 52 ºC

for 12 hours. The reaction was removed from the oil bath and allowed to cool. The vessel was placed into an ice bath and remainder of the $LiAlH_4$ was quenched by dropwise addition of diethyl ether and DI water until all the $LiAlH_4$ was neutralized. 1 M sodium hydroxide in water was then added to the TK solution to aide in the separation and extraction of the organic products from the aqueous phase. The solid byproducts of the reaction were removed by filtration using a Buchner funnel and the liquid product was transferred to a separation funnel. A water extraction in diethyl ether was used to isolate TK diol product. Sodium sulfate was then added to the TK diol solution to absorb any residual water and dried overnight. The sodium sulfate was then filtered out using a Buchner funnel and the TK diol solvents were removed using rotary evaporation. After the solvent were removed, the product was transferred to a glass vial and dried under vacuum for an additional 24 hours to ensure all solvents were removed and completely dry.

TK Diol Characterization. Nuclear magnetic resonances spectroscopy (^{1}H NMR, Bruker 400 MHz NMR) in deuterated dimethyl sulfoxide (DMSO) verified the structure of TK diol product with peaks at 1.59 ppm for the methyl group and 4.8 ppm for the hydroxyl groups. Any remaining peaks were characterized as impurities. Titration confirmed the hydroxyl (OH) number of the polyol needed to characterize its reactivity and calculate the molecular weight of the polyol. Karl Fischer titration was used to determine the percent water present in the TK diol.

nHA-LTI Grafting Reaction. nHA-LTI grafted prepolymer was synthesized by combining varying weight percent (wt%) nanocrystalline hydroxyapatite (nHA) with lysine triisocyanate (LTI) with or without the presence of iron (III) acetylacetonate (FeAA) catalyst. nHA particles were weighed out in a dry, 100 mL round bottom flask and placed in an oil bath at 80 ºC under vacuum for 48 hours to remove any residual water. The temperature was reduced to either 25 ºC or 40 ºC and purged with dry argon. LTI was added and mixed slowly by an overhead mechanical

stirrer. After fully mixed, the nHA-LTI solution was regularly sampled to assess the reaction conversion. When completed, the solution was transferred for storage under dry conditions.

Prepolymer characterization: To characterize the extent of grafting reaction between nHA-LTI, NCO number was determined at various time points using titration according to ASTM D2572-97.[26] These results were used to calculate the concentration of NCO present in the prepolymer and conversion of isocyanate and hydroxyl reactive groups during the grafting reaction. Prepolymer was dissolved in chloroform and centrifuged down to recover grafted nHA-LTI particles. X-ray photoelectron spectroscopy (XPS, Ulvac-PHI Versaprobe 5000) was utilized to determine the extent of the reaction by evaluating the presence of nitrogen and phosphorus near the surface of the nHA-LTI recovered particles.

Osteoblast mineralization assessment on nHA-PTKUR composites. Human mesenchymal stem cells (hMSCs) were maintained in mesenchymal stem cell growth medium. Cells were seeded on nHA-PTKUR composite discs along with a polymer control. After 3 days of culture on substrates, mesenchymal stem cell osteogenic differentiation medium was added to induce osteoblast differentiation. At 3, 6 and 10 days of induction, samples were washed with Dulbecco's phosphate-buffered saline (PBS), fixed with formalin (10%), and stained with alizarin red solution (2%). Stained cell layers were removed from the substrates and imaged under light microscopy. Mineralization was quantified by alizarin red staining extraction in sodium dodecyl sulfate (SDS, 5%), and absorbance measured at 405 nm.

2.4 Results

nHA-LTI grafting kinetics characterization. Nanocrystalline hydroxyapatite (nHA) was used to graft lysine triisocyanate (LTI) to create an nHA-LTI prepolymer. The extent and kinetics

of the grafting reaction were monitored primarily by NCO titration, where the relative change in percent free NCO corresponded to the conversion of free hydroxyl group on the surface on nHA particles. XPS also confirmed the presence of LTI on the surface of nHA particles after recovery of nHA-LTI grafted particles. At 40 °C, 45 wt% nHA-LTI solvent-free grafting reactions were performed with or without the addition of FeAA catalyst (**Figure 2.1A**). When monitoring grafting kinetics, both the catalyst and catalyst-free reactions prepolymer formed a crosslinked-viscous gel. The uncatalyzed prepolymer grafting reaction did not gel until day 9 while the catalyzed system gelled quickly (day 2). The experiment was repeated with thoroughly dried nHA particles, under dry inert conditions and carried out without catalyst at either 25 °C or 40 °C (**Figure 2.1B**). Under these conditions, prepolymer reactions remained relatively stable for over 1 month at both reaction temperatures, with the percent NCO dropping more quickly at elevated temperatures.

To further understand the extent of the reaction, 2nd order rate laws were utilized to model and calculate reaction rates (**Figure 2.1C**). Reaction rate, *k,* was determined by the plotting the solution to the rate law equation where [NCO] and [OH] are concentrations of reactive NCO groups and nHA surface OH groups, and C_o, $[NCO]_o$, and $[OH]_o$ are known calculated values (**Appendix A**). Reaction modeling was tested by reacting 35 wt% nHA with LTI at 40 °C under an inert, dry atmosphere. After 10 days of grafting a reaction rate, *k,* was calculated at 0.0159 $L*mol^{-1}days^{-1}$, and the experimental data was highly correlated with the 2nd model fit. (**Figure 2.1D**). Assuming an equivalent hydroxyl group concentration of 1 eq OH per 500 g nHA, based on the stoichiometric ratio, near full conversion of hydroxyl groups was achieved after 10 days of reaction (**Figure 2.1E**). The experimental rate of OH and NCO conversion also fit well with the 2nd order model (**Figure 2.1E-F**).

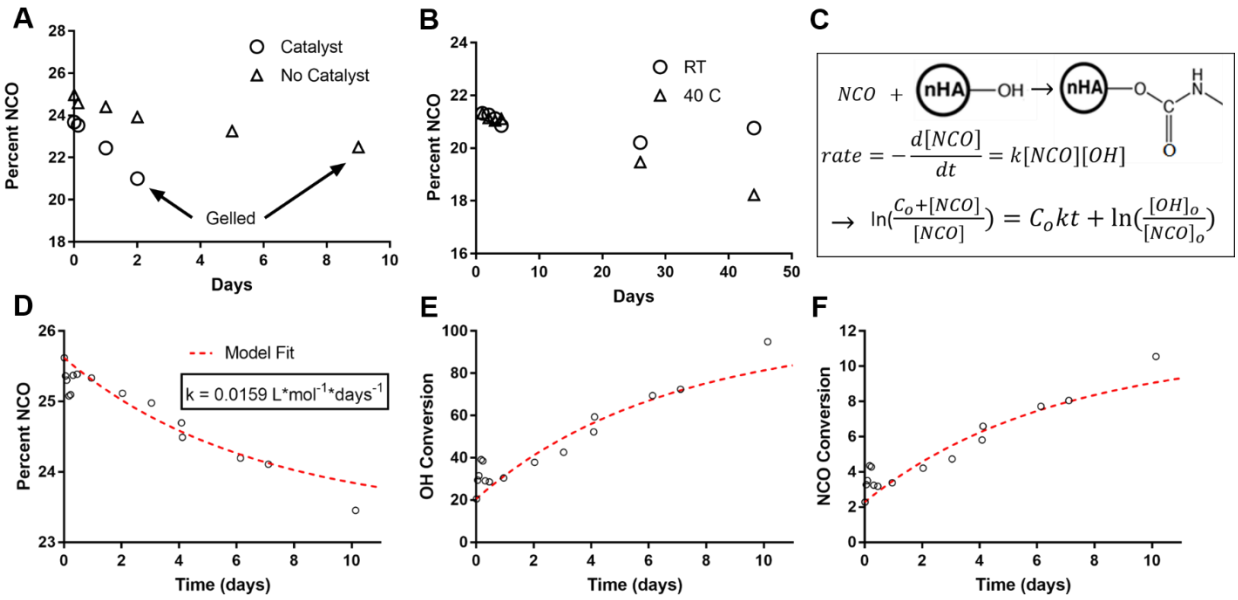

Figure 2.1: nHA-LTI grafting kinetics and modeling. (A-B) 45 wt% LTI-nHA solvent-free grafting reactions, (A) 40 °C grafting kinetic time course study with and without the addition of FeAA catalyst and (B) thoroughly dried nHA-LTI time course study without catalyst at 25 °C and 40 °C. (C) Grafting kinetic 2nd order modeling development and solution. (D-F) 35 wt% nHA-LTI grafting time course study with model overlay fit showing (D) percent NCO, (E) OH and (F) NCO conversion.

Thioketal (TK) diol scaleup and characterization. Small scale (approximately 5 g) batches of TK diol have been successfully synthesized and characterized previously in the Guelcher group.[23, 24] With the goal of producing a manufacturable product, the feasibility of scaling up TK diol production was critical. Scaleup in the lab setting, given capacity limitation was determined to be 40g batches. Following the reaction scheme outlined in **Figure 2.2A**, yields near 75% were achieved regularly allowing for batch sizes of 30 grams of TK diol to be produced in a lab setting. These procedures were translated to an industry collaborator to begin synthesizing at similar and larger batch size capabilities for the purposes of determining manufacturing feasibility.

^{1}H NMR in deuterated DMSO was primarily used to assess intermediate and final product synthesis. TK diol synthesized was verified as peaks present at 1.59 ppm for the primary methyl

group, 2.56 ppm for the primary carbon group, 3.33 ppm for the secondary carbon group, and 4.84 ppm for the hydroxyl groups. DMSO solvent peak appears at 2.50 ppm and residual water at 3.34 ppm, interfering at times with the secondary carbon group in the TK diol product (**Figure 2.2C**). All other peaks present were assumed impurities in the TK diol, likely residual reduction complexes with lithium aluminum hydride which were difficult to separate from the product. TK diol purity was assessed by calculating peak integrals and normalizing to the solvent peak integral (**Figure 2.2B**). TK diol batches initial purity was 68.3%, to increase purity, TK diol was treated in silica and Celite® columns. After treatment, purity was increased significantly to 80.0% purity for the silica treated column, but the Celite® column revealed essentially no change in purity at 68.6%. Industry collaborates produced the purest TK diol at 87% purity but were significantly burdened finically to achieve this purity level. OH number titration was also used to characterize the equivalent hydroxyl groups in TK diol. These numbers were used to calculate a molecule weight for comparison to the theoretical molecular weight of 196 g/mol. All samples tested revealed expected hydroxyl group activity and the experimentally calculated molecular weight matched the theoretical number (**Figure 2.2D**).

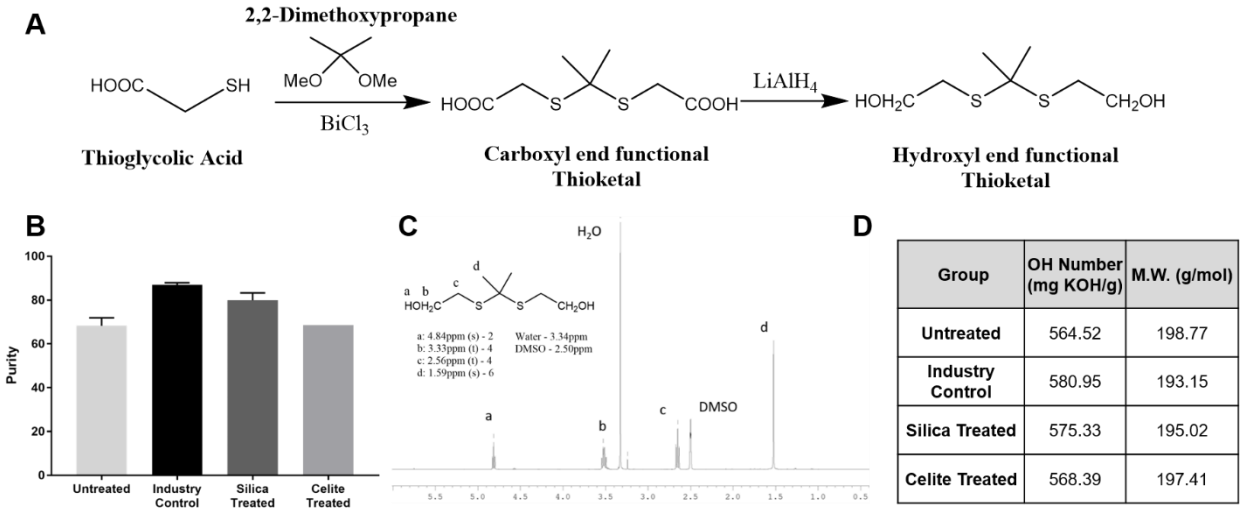

Group	OH Number (mg KOH/g)	M.W. (g/mol)
Untreated	564.52	198.77
Industry Control	580.95	193.15
Silica Treated	575.33	195.02
Celite Treated	568.39	197.41

Figure 2.2: Thioketal (TK) diol scaleup and characterization. (A) TK diol reaction scheme. (B) Purity summary results for treated and untreated PTK diol, (C) ^{1}H NMR representative spectra for structure confirmation and purity quantification. (D) OH number titration summary with theoretical value of 574 mg KOH / g sample for OH number and 196 g/mol for molecular weight.

nHA-PTKUR formulation stability and packaging configuration characterization. The storage of the nHA-PTKUR configuration was investigated as a feasibility pilot study for a long-term aging study necessary for 510(k) FDA submission. Stability of both the prepolymer and TK diol were tested in preliminarily chosen packaging solutions. Dual barrel (DB) syringes with a static mixing head allow for the PTKUR bone graft to be an injectable, settable product. Pre-packing into DB syringes is the ideal solution as the product can be stored in a "ready-to-use" form allowing a surgeon to pick up the product and use it immediately. Sulzer brand K-series DB syringes (DB syringe 1) were chosen as the initial candidate and were provided by Medtronic Inc. (**Figure 2.3E**). Burst pouches provide a similar mechanism but require mechanical mixing within the pouch before injection of the bone graft. Both packaging solutions were tested in a pilot, 2-week stability study at elevated temperature (40 °C) to accelerate aging affect.

NCO titration and XPS was performed on the prepolymer to assess stability in the DB syringe 1, the burst pouch and bulk storage (glass vial). Percent NCO for all groups decreased over the 2-week time course (**Figure 2.3A**). The prepolymer was expected to drift downward in percent NCO as the reaction may continue to proceed during storage, especially at elevated temperature. The DB syringe drifted down about 0.5 percent NCO, while the burst pouch decreased near 1 percent NCO over two weeks. The bulk storage group also decreased, suggesting a prepolymer stability issue rather than a packaging issue. XPS was performed to assess nitrogen to phosphorus ratios in the prepolymer over time (**Figure 2.3B**). Given large error discrepancy within XPS testing, all groups measured an N:P ratio near 1.5, which is near the theoretical value (2 mol N: 1 mol P on the surface of the nHA-LTI particle).

OH number and Karl Fischer titration on TK diol were used to assess the stability of the polyol-phase of the PTKUR precursor. OH number for all storage solutions and time points were stable and within the theoretical and previously reported ranges (574 mg KOH per g) (**Figure 2.3C**). [24] Karl Fischer titration was performed on the TK diol to determine the percent water. TK diol processing includes a water extraction to clean and effectively separate the compound from impurities, so it is anticipated that residual water will be present in the final product. TK diol is thoroughly dried after synthesis as residual water will affect the OH number and hydroxyl activity during PTKUR formation. Karl Fischer titration showed minimal water (<1% water) for all measurements (**Figure 2.3D**). The bulk measurements were notably higher than all other measurements but can be explained as the bulk TK diol was measured from a different TK diol batch. These data suggest while the percent water was low overall, there is high batch to batch variability in percent residual water in TK diol.

A third storage solution was chosen from Nordson EFD and provided again by Medtronic Inc. for further testing (DB Syringe 2) (**Figure 2.3E**). Prepolymer stability was further tested by NCO titration using dried nHA-LTI prepolymer in a time course study. A two-month stability study was performed using all three storage solutions under accelerated aging condition of 40 °C. The kinetic modeling discussed previously was utilized to help understand reaction kinetics under storage conditions. It is notable that under storage conditions, reaction rates are expected to be slow without agitation or mixing occurring. Percent NCO trended downward over the course of two months for all three storage solutions (**Figure 2.3F**). Both DB syringes drifted down nearly 2 percent NCO by two months, and the kinetic model closely followed the experimental measurements. The burst pouch decreased over 2 percent NCO in two weeks and had formed a crosslinked gel by the two-month time point. OH conversion for all three groups trended upwards over the 2 month time course, with the burst pouch reaching almost total OH conversion by two weeks (**Figure 2.3G**). A long-term aging study (1 year) was simultaneously started to evaluate the fundamental storage kinetics in well-sealed glass vials at room temperature (25 °C) and elevated temperature (40 °C) (**Figure 2.3H**). The reaction kinetics tracked similarly to the 2-month stability study, and by 4 months the well-sealed prepolymer had also formed a crosslinked gel. This revealed fundamental problems with the prepolymer stability long-term, and suggests this product may not be capable of a long-term shelf life.

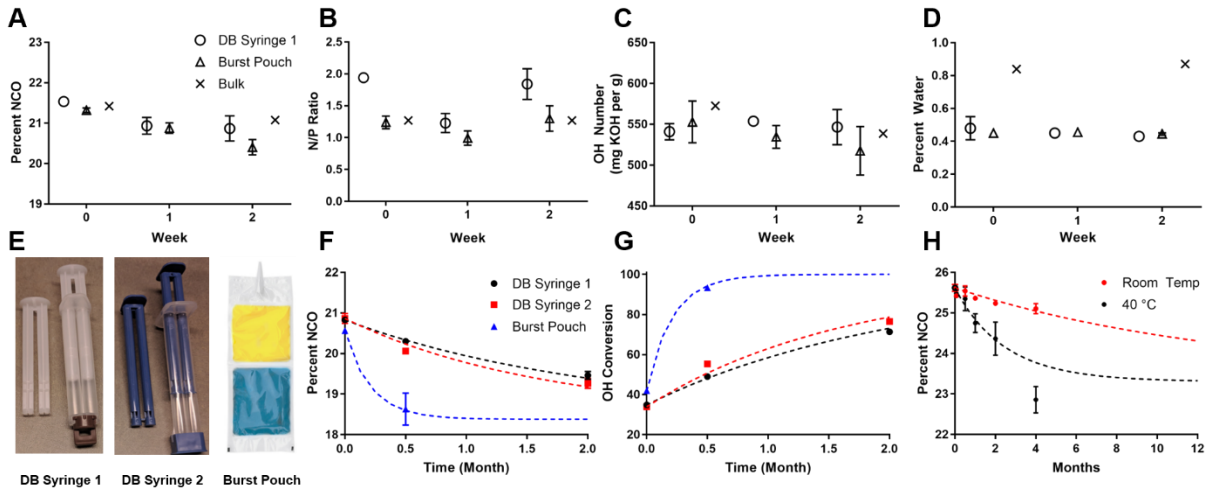

Figure 2.3: nHA-PTKUR formulation stability and packaging configuration characterization. (A-D) Stability study investigating (A-B) nHA-LTI prepolymer and (C-D) TK diol packaging and aging stability by (A) percent NCO, (B) XPS nitrogen/phosphorus (N/P) ratio, (D) percent water by Karl Fischer titration. (E) Packaging configuration investigated. (F-H) Further investigation into prepolymer stability with nHA-LTI prepolymer grafting model overlay showing (F) percent NCO, (G) OH conversion and (H) long-term percent NCO at 25 °C and 40 °C.

nHA-PTKUR bone graft mineralization assessment. To assess osteogenic and mineralization cellular response of the nHA-PTKUR bone graft, mineralization assays were performed *in vitro*. Alizarin red staining was used to visualize osteoblast mineralization occurring on PTKUR bone graft discs and quantified as absorbance at 405 nm. Three groups were synthesized to assess nHA wt% loading on cellular response 0 %wt nHA polymer controls, 34 wt% and 45 wt% nHA. 34 wt% nHA-PTKURs were examined as 34 wt% nHA corresponds to a 1:1 volume ratio of nHA-LTI prepolymer to TK diol for use in DB syringes. All groups trended upwards in mineralization response throughout the time course study. The 45 wt% nHA-PTKUR group had the greatest cellular response but leveled out by day 6. While the 34 wt% group was lower than the 45 wt% group, these data show significantly higher cellular response than the polymer control disc (**Figure 2.4C**). Visually all groups showed significant uptake of alizarin red

staining suggesting lower nHA loading wt% will not affect the cellular response *in vivo*, especially if there are significant benefits from a manufacturing perspective to create a 1:1 volume ratio for the creation of a simplistic and "easy to use" product (**Figure 2.4A-B**). Notably, with lower nHA loading in the prepolymer, this is anticipated to affect the mechanical properties of the PTKUR and would need to be tested further if this were to be implemented.

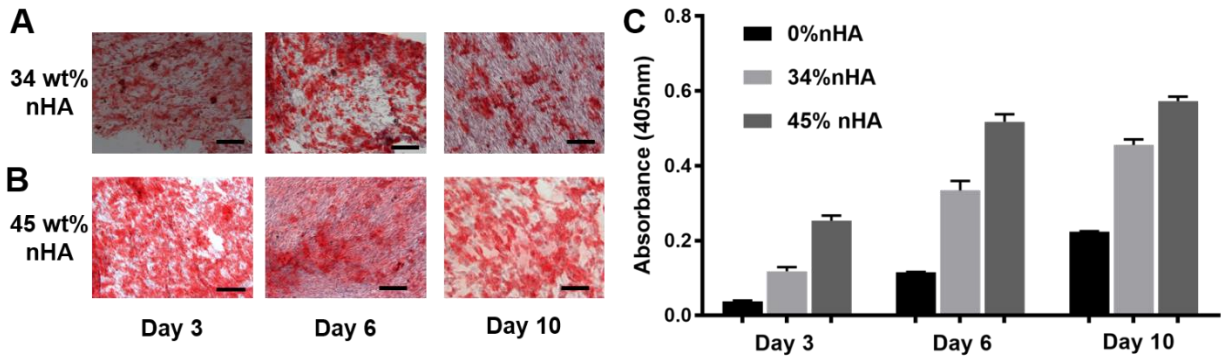

Figure 2.4: Osteoblast mineralization on nHA-PTKUR bone grafts. (A-B) Alizarin red staining of human mesenchymal stem cells (hMSCs) cultured on (A) 34 wt% and (B) 45 wt% nHA-LTI based PTKUR composites at day 3, 6 and 10 (C) Quantification of alizarin red staining by extraction of the dye and absorbance measured at 405 nm (Scale bar: 200 μm)

2.5 Discussion

In this work, nHA-PTKUR precursors and final products were investigated and tested primarily as a feasibility study for an eventual FDA submission under a 510(k) showing equivalency to current products on the market, such as Medtronic's Infuse Bone Graft™ or similar products. This work leads into an *in vivo* investigation discussed in Chapter 3 of the PTKURs in a pre-clinical rabbit femoral condyle defect model to assess bone graft performance. These data together work to produce a product on track for clinical use.

Prepolymer synthesis, characterization and stability represented a large technical challenge and barrier. Early work in nHA-LTI grafting studies concluded that quickly grafting a prepolymer

with FeAA catalyst were sufficient for synthesis.[20] Yet as kinetics and stability of the grafting reaction was further investigated, challenges with competing reactions and crosslinking-gelation became an issue. Initial time course studies resulted in prepolymer viscosity buildup and eventual gelation. We initially hypothesized this was due to a competing reaction occurring during the prepolymer synthesis, such as an allophanate reaction, which generally occurs at much higher temperatures or with catalyst.[27, 28] Other concerns included presence of water adsorbed onto the nHA particles, or water from the environment inferring with the reaction during sampling. Either competing allophanate reactions or water contamination would lead to percent NCO decreasing overtime and would explain long-term decreases in percent NCO and eventual prepolymer gelation. These concerns were addressed by drying nHA particles thoroughly prior to reaction, removing catalyst, and reducing heat. While these changes initially helped create more stable prepolymer and prevented gelation, long-term studies revealed percent NCO drift still occurred.

Second order kinetic modeling aided in predicting prepolymer percent NCO performance over time, but eventually all prepolymer formulation drifted below acceptable limits when stored under accelerated aging conditions. Taken overall, these data suggest the prepolymer formulation may not be suitable for long-term storage as the drift in percent NCO will affect the indexing of the PTKUR bone graft. Prepolymers necessary for PTKUR will need to be made and used rapidly after manufacturing, which will undoubtably add high cost and logistical difficulties, potentially precluding its use.

Recent work in prepolymer synthesis suggest some of these challenges may be overcome by first thoroughly washing nHA particles in solvents such as tert-butyl-methyl ether (TBME) or 2-propanol prior to use. nHA particles of diameters near 200 nm are created using various surfactants based emulsions.[29, 30] While these surfactants are washed away by manufacturers, trace

amounts may still be present especially in these nano-scale, high surface area particles with high surface binding energy. These trace amounts may be responsible for long-term stability issues as these chemicals could react with LTI over time. If so, thoroughly washing nHA particles should be investigated as a potential solution to overcome this technical challenge.

An equally challenging technical problem proved to be the scaleup and technological transfer of the TK diol to a manufacturing setting. Batch to batch variability in purity and water uptake were the primary challenges to overcome. With this high variability, creating industry specifications for this precursor was challenging. In a lab setting, TK diol purity could be increased by treating with a silica gel column, but when scaling up in a manufacturing setting, this adds huge costs and feasibility issues when increasing batch sizes to kilo-scale. A ^{1}H NMR spectra peak integration was utilized as a purity assay in lab, but a gas chromatography-mass spectrometry (GC-MS) or similar assessment needs to be developed to accurately assess purity to create a more legitimate specification for use in a good manufacturing practice (GMP) certified setting.

When TK diol was tested in the preliminary 2-week stability study, the product performed well, revealing long-term storage will not present a challenge. Both the OH number and Karl Fischer titration showed favorable results moving towards a long-term aging study. The prepolymer side did not perform well and these short-term stability studies were repeated with similar results. Still, the DB syringe packaging configurations both proved to be sufficient and promising for future use of an injectable PTKUR bone graft. While the prepolymer percent NCO drifted in the DB syringes, further studies in well-sealed glass vials showed this was an issue with the prepolymer formulation, not the packaging configurations. If the prepolymer problem can be overcome, DB syringes, especially at a 1:1 volume ratio, in either the Sulzer or Nordsom syringes can be used for injecting, mixing and creating a settable bone graft *in situ.* The burst pouch did not

perform well in the 2-week or the 2-month stability study. This could be due to prepolymer exposure to an unknown, trade-secret thin-film separating each side prior to mixing. This chemical could adversely react with the prepolymer and cause stability issues. The large drop NCO and gelation of the prepolymer seen in the 2-month stability study was particularly concerning. The prepolymer was thoroughly protected from all environmental factors, such as exposure to humidity, and under the exact same conditions as the DB syringes and failed to maintain prepolymer stability. This suggests the burst pouches should not be used as a long-term packaging configuration, even with the existing issues of the prepolymer.

The alizarin red mineralization assay results suggested the 34 wt% nHA-PTKUR bone graft was acceptable for use, from a cellular response perspective. While cellular activity and positive staining for mineralization was not as significant as the 45 wt% group, there is preliminary, unpublished work suggesting osteoblast mineralization *in vivo* is not highly correlated to nHA loading. The exact lower limit of nHA loading remains unknown, but 34 wt% nHA loading appears to be above the threshold based on this study. This is important from the perspective of creating a 1:1 volume ratio in the DB syringes. While custom syringes can be created to adjust for varying volume, these syringes are costly and would likely preclude the use of this product from a financial perspective.

2.6 Conclusion

nHA-PTKUR bone grafts are an attractive new technology in the forefront of biomaterials. The cell-degradable polymer, combined with the osteogenic and mechanically favorable properties of nHA ceramics, represents a promising product for FDA submission. This work begins the process for screening and overcomes technological challenges which are inevitable in the new

product development phase. We have shown promising solutions to prepolymer formulation, TK diol synthesis, and packaging configuration for the next phase of development. Chapter 3 will look further into this family of nHA-PTKUR products and establish preclinical animal model testing in a rabbit femoral condyle defect model.

2.7 References

1. Khan, Y.; Yaszemski, M. J.; Mikos, A. G.; Laurencin, C. T., Tissue engineering of bone: material and matrix considerations. *J Bone Joint Surg Am* **2008,** *90 Suppl 1*, 36-42.
2. Parikh, S., Bone graft substitutes: past, present, future. *Journal of postgraduate medicine* **2002,** *48* (2), 142.
3. Schmidt-Bleek, K.; Kwee, B. J.; Mooney, D. J.; Duda, G. N., Boon and Bane of Inflammation in Bone Tissue Regeneration and Its Link with Angiogenesis. *Tissue Eng Part B Rev* **2015,** *21* (4), 354-64.
4. Younger, E. M.; Chapman, M. W., Morbidity at bone graft donor sites. *J Orthop Trauma* **1989,** *3* (3), 192-195.
5. Wagoner Johnson, A. J.; Herschler, B. A., A review of the mechanical behavior of CaP and CaP/polymer composites for applications in bone replacement and repair. *Acta Biomaterialia* **2011,** *7* (1), 16-30.
6. Bohner, M., Design of ceramic-based cements and putties for bone graft substitution. *Eur Cell Mater* **2010,** *20*, 1-12.
7. Guda, T.; Walker, J. A.; Pollot, B. E.; Appleford, M. R.; Oh, S.; Ong, J. L.; Wenke, J. C., In vivo performance of bilayer hydroxyapatite scaffolds for bone tissue regeneration in the rabbit radius. *Journal of Materials Science: Materials in Medicine* **2011,** *22* (3), 647-656.
8. Hing, K. A., Bioceramic Bone Graft Substitutes: Influence of Porosity and Chemistry. *International Journal of Applied Ceramic Technology* **2005,** *2* (3), 184-199.
9. Lovati, A. B.; Lopa, S.; Recordati, C.; Talò, G.; Turrisi, C.; Bottagisio, M.; Losa, M.; Scanziani, E.; Moretti, M., In Vivo Bone Formation Within Engineered Hydroxyapatite Scaffolds in a Sheep Model. *Calcified Tissue International* **2016**, 1-15.
10. Adhikari, R.; Gunatillake, P. A.; Griffiths, I.; Tatai, L.; Wickramaratna, M.; Houshyar, S.; Moore, T.; Mayadunne, R. T.; Field, J.; McGee, M.; Carbon, T., Biodegradable injectable polyurethanes: synthesis and evaluation for orthopaedic applications. *Biomaterials* **2008,** *29* (28), 3762-3770.
11. Adolph, E. J.; Hafeman, A. E.; Davidson, J. M.; Nanney, L. B.; Guelcher, S. A., Injectable polyurethane composite scaffolds delay wound contraction and support cellular infiltration and remodeling in rat excisional wounds. *J Biomed Mater Res A* **2012,** *A100A*, 450-61.
12. Bonzani, I. C.; Adhikari, R.; Houshyar, S.; Mayadunne, R.; Gunatillake, P.; Stevens, M. M., Synthesis of two-component injectable polyurethanes for bone tissue engineering. *Biomaterials* **2007,** *28* (3), 423-433.
13. Nagata, M.; Oi, A.; Sakai, W.; Tsutsumi, N., Synthesis and properties of biodegradable network poly (ether-urethane) s from L-lysine triisocyanate and poly (alkylene glycol) s. *Journal of Applied Polymer Science* **2012,** *126* (S2).
14. Storey, R. F.; Wiggins, J. S.; Puckett, A., Hydrolyzable poly (ester-urethane) networks from l-lysine diisocyanate and d, l-lactide/ϵ-caprolactone homo-and copolyester triols. *Journal of Polymer Science Part A: Polymer Chemistry* **1994,** *32* (12), 2345-2363.
15. Dumas, J. E.; Brownbaer, P. B.; Prieto, E. M.; Guda, T.; Hale, R. G.; Wenke, J. C.; Guelcher, S. A., Injectable reactive biocomposites for bone healing in critical-size rabbit calvarial defects. *Biomed Mater* **2012,** *7* (2), 024112.
16. Guelcher, S. A.; Patel, V.; Gallagher, K. M.; Connolly, S.; Didier, J. E.; Doctor, J. S.; Hollinger, J. O., Synthesis and In Vitro Biocompatibility of Injectable Polyurethane Foam Scaffolds. *Tissue Engineering* **2006,** *12* (5), 1247-59.

17. Guelcher, S. A.; Srinivasan, A.; Dumas, J. E.; Didier, J. E.; McBride, S.; Hollinger, J. O., Synthesis, mechanical properties, biocompatibility, and biodegradation of polyurethane networks from lysine polyisocyanates. *Biomaterials* **2008,** *29* (12), 1762-1775.
18. Hafeman, A. E.; Zienkiewicz, K. J.; Zachman, A. L.; Sung, H.-J.; Nanney, L. B.; Davidson, J. M.; Guelcher, S. A., Characterization of the degradation mechanisms of lysine-derived aliphatic poly (ester urethane) scaffolds. *Biomaterials* **2011,** *32* (2), 419-429.
19. Page, J. M.; Prieto, E. M.; Dumas, J. E.; Zienkiewicz, K. J.; Wenke, J. C.; Brown-Baer, P.; Guelcher, S. A., Biocompatibility and chemical reaction kinetics of injectable, settable polyurethane/allograft bone biocomposites. *Acta Biomater* **2012,** *8*, 4405-4416.
20. Lu, S.; McGough, M.; Rogers, B.; Wenke, J.; Shimko, D.; Guelcher, S., Resorbable nanocomposites with bone-like strength and enhanced cellular activity. *Journal of Materials Chemistry B* **2017,** *5* (22), 4198-4206.
21. Webster, T. J.; Ergun, C.; Doremus, R. H.; Siegel, R. W.; Bizios, R., Enhanced functions of osteoblasts on nanophase ceramics. *Biomaterials* **2000,** *21* (17), 1803-1810.
22. Lu, S.; McGough, M. A.; Shiels, S. M.; Zienkiewicz, K. J.; Merkel, A. R.; Vanderburgh, J. P.; Nyman, J. S.; Sterling, J. A.; Tennent, D. J.; Wenke, J. C., Settable polymer/ceramic composite bone grafts stabilize weight-bearing tibial plateau slot defects and integrate with host bone in an ovine model. *Biomaterials* **2018**.
23. Martin, J. R.; Gupta, M. K.; Page, J. M.; Yu, F.; Davidson, J. M.; Guelcher, S. A.; Duvall, C. L., A porous tissue engineering scaffold selectively degraded by cell-generated reactive oxygen species. *Biomaterials* **2014,** *35* (12), 3766-3776.
24. McEnery, M. A.; Lu, S.; Gupta, M. K.; Zienkiewicz, K. J.; Wenke, J. C.; Kalpakci, K. N.; Shimko, D. A.; Duvall, C. L.; Guelcher, S. A., Oxidatively degradable poly (thioketal urethane)/ceramic composite bone cements with bone-like strength. *RSC advances* **2016,** *6* (111), 109414-109424.
25. Yu, S. S.; Koblin, R. L.; Zachman, A. L.; Perrien, D. S.; Hofmeister, L. H.; Giorgio, T. D.; Sung, H.-J., Physiologically Relevant Oxidative Degradation of Oligo(proline) Cross-Linked Polymeric Scaffolds. *Biomacromolecules* **2011,** *12* (12), 4357-4366.
26. International, A., Standard test method for isocyanate groups in urethane materials or prepolymers. ASTM International: 2010.
27. Lapprand, A.; Boisson, F.; Delolme, F.; Méchin, F.; Pascault, J. P., Reactivity of isocyanates with urethanes: Conditions for allophanate formation. *Polymer Degradation and Stability* **2005,** *90* (2), 363-373.
28. Heintz, A. M.; Duffy, D. J.; Hsu, S. L.; Suen, W.; Chu, W.; Paul, C. W., Effects of reaction temperature on the formation of polyurethane prepolymer structures. *Macromolecules* **2003,** *36* (8), 2695-2704.
29. Lim, G.; Wang, J.; Ng, S.; Gan, L., Formation of nanocrystalline hydroxyapatite in nonionic surfactant emulsions. *Langmuir* **1999,** *15* (22), 7472-7477.
30. Uota, M.; Arakawa, H.; Kitamura, N.; Yoshimura, T.; Tanaka, J.; Kijima, T., Synthesis of High Surface Area Hydroxyapatite Nanoparticles by Mixed Surfactant-Mediated Approach. *Langmuir* **2005,** *21* (10), 4724-4728.

CHAPTER 3

INTRAMEMBRANOUS AND ENDOCHONDRAL REMODELING OF NANOCRYASTALLINE HYDROXYAPATIE-POLY(THIOKETAL URETHANE) BONE GRAFTS IN A RABBIT FEMORAL CONDYLE DEFECT MODEL

3.1 Abstract

Polyurethanes (PURs) are an attractive material for tissue engineering bone graft substitutes since they can be formulated to be injectable, settable, and biocompatible, and their mechanical properties and degradation rates can be tuned for specific orthopedic applications. Recently, a novel poly(thioketal urethane) (PTKUR) bone graft was developed to address unpredictable resorption associated with hydrolytic degradation of ester groups in poly(ester urethane) bone grafts *in vivo*. In the present study, nanocrystalline hydroxyapatite (nHA) was incorporated with PTKUR to exploit the osteogenic and mechanical benefits of nHA in a polymeric nHA-PTKUR bone graft. nHA was grafted with lysine triisocyanate (LTI) to enhance nHA dispersion in a lysine-based nHA-PTKUR hybrid polymer that exhibits a complementary combination of cell-mediated resorption mechanisms as PTKUR degrades by ROS and nHA is resorbed by osteoclasts that release ROS. nHA-PTKUR "glue," without inorganic filler particles, incorporated 25 vol% nHA, degrades rapidly in oxidative conditions, and remains stable in hydrolytic conditions. Mechanical analysis revealed a modulus of 370 MPa and ultimate strength of 53 MPa. nHA-PTKUR "putties" (14 vol% nHA) contained 45 wt% Calcium Phosphate (CaP), 10 wt% CaP/35 wt% sucrose porogen, or 45 wt% sucrose to explore the addition of slowly-degrading, mechanically robust, and osteoconductive CaP particles and porosity on mechanical properties and remodeling *in vivo*. nHA-PTKUR glue and putties demonstrated cellular infiltration, a combination of endochondral and intramembranous bone formation, and new

calcified bone within femoral condyle defects as early as four months. This work represents a critical step towards the development of a nHA-PTKUR bone graft with potential application in weight-bearing defects.

3.2 Introduction

Previous work has demonstrated the advantages of lysine-based poly(ester urethane) (PEUR) as a settable, tissue engineering bone graft.[1-10] These PEURs undergo autocatalytic degradation in hydrolytic environments leading to unpredictable resorption that may not match patient biology.[7, 11] Our group has previously worked with a poly(thioketal urethane) (PTKUR) to overcome the shortcomings of PEURs. A novel thioketal (TK) diol was synthesized for fabrication of a hydrolytically stable PTKUR that undergoes oxidation of the lysine and TK residues in the presence of cell-generated reactive oxygen species (ROS). PTKURs demonstrated bone-like strength and histological analysis showed evidence of osteoclast-mediated resorption of the cements at 6 and 12 weeks *in vivo*.[12]

Hydroxyapatite (HA) makes up 50-70% of native bone making it another attractive bone graft substitute.[13-18] Nanocrystalline hydroxyapatite (nHA) in particular has been shown to stimulate new bone formation by enhancing osteoblastic differentiation compared to micron-scale hydroxyapatite.[19, 20] Polyurethane/nHA composite bone grafts have been proposed to take advantage of the properties of the two components.[21-23] However, despite the inherent strength of HA, limited HA-polymer bonding and HA aggregation generally decrease the mechanical properties of these composites.[13] To overcome this, the surface hydroxyl (OH) groups of nHA can be grafted with isocyanates (NCO) for NCO-grafted nHA prepolymer and synthesis of nHA-PUR hybrid polymers.[19, 22, 24-26] Previously, we presented enhanced dispersion of lysine triisocyanate

grafted nHA (nHA-LTI) in nHA-LTI-PEUR nanocomposites synthesized from nHA-LTI/LTI prepolymer and PCL triol (MW=300). LTI grafting yielded compressive properties and bending strengths suitable for weight-bearing applications and *in vitro* studies demonstrated enhanced mineralization compared with nHA-PEUR nanocomposites in which the nHA was not grafted in a prepolymer step.[19] Furthermore, nHA-LTI-PEUR nanocomposites incorporating 55 wt% CaP particles mechanically stabilized un-instrumented tibial plateau defects in sheep and supported remodeling and osteogenesis at 16 weeks.[25]

In this study, the osteogenic properties of nHA were combined with the bulk material properties of PTKURs in a new class of settable nHA-PTKUR hybrid polymer synthesized by the reaction of nHA-LTI/LTI prepolymer and TK diol. A complementary combination of cell-mediated resorption mechanisms was anticipated as PTKUR degrades by ROS and nHA is resorbed by osteoclasts that release ROS.[12, 27-29] The bulk material properties were characterized prior to implantation in a rabbit femoral condyle defect model. The material was also tested in a small notch defect in the tibial diaphysis to investigate persistence of the nHA-PTKUR bone graft in a non-critical defect. These studies were carried out to 18 months to explore cellular infiltration, differentiation of osteoprogenitor cells, and nHA-PTKUR resorption long-term. The addition of CaP particles and two ranges of sucrose porogen is also investigated to determine the effects of slowly degrading CaP and porosity on mechanical properties and remodeling *in vivo*.

3.3 Materials and Methods

Materials. All reagents for thioketal (TK) diol synthesis, iron (III) acetylacetonate (FeAA) catalyst, ε-caprolactone, and sucrose were purchased from Sigma Aldrich. FeAA was dissolved in dry ε-caprolactone (5% w/w) prior to use for a flowable, low concentration catalyst solution.

Lysine triisocyanate (LTI) was purchased from Jinan Haohua Industry Co., LTD (Jinan, China) and carbon treated in tert-butyl-methyl ether (TBME, Acros Organics) prior to use.[12, 19, 25] Nanostim™ Synthetic Bone Paste (NS) and ceramic calcium phosphate (CaP) particles were provided by Medtronic (Memphis, TN). Upon receipt, particles were ground to 100-300 μm, washed with acetone and water, and dried under vacuum (100 °C).[12]

Hydroxyapatite dewatering. Nano-scale hydroxyapatite (nHA) was isolated from the NS suspension for use in nHA-PTKUR synthesis. Approximately 5 cc NS was dispensed into a 50 mL centrifuge tube. The centrifuge tube was filled with 40 mL 2-propanol and the mixture vortexed until the NS suspension was dispersed in the solvent. The nHA was separated using centrifugation and the process was repeated 3 times. The isolated nHA pellet was dried under vacuum overnight and then under vacuum at 80 °C for at least 24 hours. The dry pellet was morselized to nano-scaled particles using a mortar and pestle. The nHA was re-dried for at least 48 hours at 80 °C immediately prior to use. Dry material was sent to Micromeritics Analytical Services for analysis. The density and surface area were evaluated by gas displacement (helium) and the BET method according to ISO 9277, respectively.[30]

Hydroxyapatite surface modification. nHA was grafted with polycaprolactone (PCL-g-nHA) or LTI (LTI-g-nHA) for the diol and isocyanate phases, respectively, adapting methods described previously.[19, 25, 31] Dry ε-caprolactone was charged to a three-neck boiling flask containing dry nHA particles (3.7:1) and equipped with a condenser. The reaction was stirred for 24 hours at 150 °C. Grafted particles were recovered from excess ε-caprolactone by sonicating with chloroform four times. PCL grafted nHA was dried under vacuum at 80 °C overnight. LTI was grafted to the surface of nHA by combining dry nHA particles with LTI (1:1) and mixing for 1 minute (FlackTek SpeedMixer, DAC 150 FVZ-K). FeAA catalyst solution (0.5 % w/w) was

added and the suspension mixed at maximum speed for a total of 10 minutes. Surface modified particles were washed from excess LTI and catalyst with TBME. Clean LTI-g-NS was dried under vacuum. TGA (Instrument Specialist's TGA-1000) was performed to verify grafting onto the surface of NS nHA particles by thermal stability analysis. XRD (Rigaku SmartLab X-Ray Diffractometer, $\lambda = 0.154$ nm) was conducted to verify no change in crystallinity of the grafted NS-g-PCL and NS-g-LTI particles as previously published.[19] Average 2θ (radians) peak analysis was performed for calculations of average grain size for NS and NS grafted particles.[32]

Nano-scale hydroxyapatite thioketal synthesis. A TK diol was synthesized as described in the previous chapter.[12] Briefly, 2,2-dimethoxypropane was reacted with thioglycolic acid in acetonitrile for 24 hours at room temperature. The intermediate was filtered and the solvent removed. Dry intermediate was dissolved in tetrahydrofuran and added to lithium aluminum hydride in diethyl ether dropwise in an ice bath. The reaction was refluxed at 52 °C overnight and the product extracted. The product was dried under vacuum for at least 48 hours to ensure all solvents were removed. FeAA catalyst was dissolved in the TK diol (for total of 0.125 wt% FeAA in nHA-PTKUR material for composite putties or 0.0625% for nHA-PTKUR glue) on a stir plate overnight. The catalyzed TK was then blended 1:1 with dry PCL-g-NS and mixed until homogeneous (about 5 minutes) using a speed mixer and stored at 4 °C until needed.

nHA-LTI prepolymer synthesis. The prepolymer was synthesized according to methods published previously.[19, 25] Dry, LTI-g-NS was ground with a mortar and pestle to ensure nano-scale powder. Then, HA was added to a mixing cup followed by the addition of LTI for 40 wt% LTI-g-NS in LTI. The mixture was mixed in 1 minute intervals using a speed mixer until homogeneous (about 5 minutes). The NCO number was verified by NCO titration.[33]

NS-LTI grafting reaction. Prepolymer grafting kinetics were assessed by reacting NS with LTI and measuring the percent free isocyanate by titration. Briefly, 35 wt% NS was added to a 100 mL 3-neck flask and dried under vacuum at 80 °C for 48 hours. Temperature was reduced to 40 °C and LTI was added without catalyst under an inert atmosphere and stirred with an overhead mechanical stirrer. Samples were taken periodically to monitor the reactions conversion. The conversion of NCO and OH groups were calculated and modeled using 2nd order reaction kinetics.

nHA-PTKUR fabrication and characterization. Remodeling of a settable nHA-PTKUR hybrid polymer bone graft was investigated with and without porogen and CaP. All formulations were fabricated by first blending catalyzed nHA-PTKUR and nHA-LTI at an NCO:OH index of 140 for composites and 120 for nHA-PTKUR glue. The lower index of the glue was chosen to achieve approximately equal volumes of nHA-LTI and nHA-PTKUR. The solids (CaP ± sucrose) were then added and mixed by hand until homogeneous, about 30 seconds. The material was molded or loaded into a syringe for the desired delivery method. The materials were cured overnight in cylindrical tubes (6 mm diameter) for characterization. Cured samples were then leached in water at 37 °C for 5 days to ensure all sucrose was removed. Samples without solids were γ-irradiated at a dose of 25 kGY and sent NAMSA® for cytotoxicity testing to ensure nHA-PTKUR biocompatibility. There, *in vitro* cytotoxicity testing was performed according to ISO 10993-5 under an ISO 13485 certified Quality System with the test method accredited to ISO 17025.

Mechanical characterization. Quasi-static compression testing was performed on all groups to quantify the mechanical characteristics and investigate the mechanical consequences of sucrose addition.[12, 34, 35] Leached cylindrical samples were cut to a height of 12 mm (2X diameter) using an IsoMet Low Speed Saw to ensure flat, parallel edges. The samples were compressed between circular plates at a rate of 25 mm/min and the force and displacement recorded (MTS 858

Bionix Servohydraulic Test System). Engineering stress and strain were calculated and used to determine the modulus, and maximum stress and yield strain for each material.

nHA-PTKUR in rabbits. All surgical and care procedures were carried out at IBEX Preclinical Research, Inc. (Logan, UT) under aseptic conditions per the approved IACUC protocol. nHA-PTKUR putties containing 45 wt% CaP (45C0S group), 35 wt% sucrose plus 10 wt% CaP (10C35S group), or 45 wt% sucrose (0C45S group), and an nHA-PTKUR "glue" without solids (0C0S group) were implanted in bilateral cylindrical defects (5 mm Ø x 8 mm) in the distal femoral condyles of rabbits. Unilateral slot defects (10 mm length x 2 mm) were also created in the right tibia and filled with the 0C0S material or left empty as a control. Each rabbit received a different graft in each femur for n=3 for each group at each time point. Animals were sacrificed at 4, 12 and 18 months. The femurs and tibias were harvested and fixed in 10% formalin.

In vivo analysis. While in formalin, the bones were scanned with a voxel size of 17.2 μm using a μCT 50 (Scanco). 2D images were taken at the center of the defect and the defect length and width measured using ImageJ. The length/width of the graft was measured at three different points on the graft and an average reported for each specimen (**Figure 3.4C-D**). Bone volume percent (BV/TV) was quantified for three concentric, annular cylinders ("rings") with a width of 0.8 mm and a central core cylinder with a radius of 0.8 mm (**Figure 3.4A**). The cylinders were morphed to a length encompassing the center 5 mm of the defect. Theoretically, the inner bound of Pipe 1 is at the interface of the defect and the host-bone and consists of mostly host bone. A constant analysis threshold was maintained for all groups (**Figure 3.4B**). Calcified specimens were processed and plastic-embedded by Histion. Sections were taken from the center of the defect, ground to 30-70 μm, and stained with Stevenel's Blue for histological analysis. Methods described previously were adapted for quantitative histomorphometry.[25] A 2 mm x 8 mm rectangle was

created 2 mm from the insertion of the cylindrical defect. The rectangle was divided into 8 smaller rectangles that were 1 mm x 2 mm to compare staining at various regions from the host-bone, host-bone/defect interface and within the defect at 4, 12, and 18 months (**Figure 3.7**). The distal 4 regions were included in analysis since the marrow space will introduce significant error. Sections from each group were also stained with Safranin O and Fast green which better distinguishes cartilage and bone.

Collagen 10 IHC Staining. Polished sections were washed with Tween^{TM} phosphate buffer saline (PBS). Heat-mediated antigen retrieval was performed with citrate buffer at 80 °C for 1 hour followed by a PBS wash. Samples were then treated in 0.5% H_2O_2 for 10 minutes and washed with PBS. Samples were blocked in 5% goat serum for 1 hour and incubated with anti-Collagen 10 antibody (1:1000) overnight at 4 °C followed by incubation in goat anti-mouse-HRP secondary antibody (1:500) for 1 hour at room temperature. Collagen 10 expression was detected with NovaRed Chromagen Kit following the manufacturer's directions

Statistical methods. All data is reported as the average ± standard deviation unless otherwise specified. A one-way ANOVA (GraphPad Prism) with a post-hoc Tukey Test was used to test for significance of mechanical properties. A Student's t-Test was performed to detect differences in defect length with time for a given material group. A two-way ANOVA with a post-hoc Tukey Test was used to investigate differences in BV/TV for each pipe at the various time points for each material. BV/TV could not be compared between the different materials as common thresholding could not distinguish HA materials between the groups. A two-way ANOVA was also performed on histomorphometry data with a post-hoc Sidak's multiple comparisons test. Histomorphometry is plotted with standard error of the mean (SEM).

3.4 Results

nHA-PTKUR characterization. NS nHA was used to synthesize nHA-PTKUR. After de-watering, NS particles were short fibers with a width of 20 nm, yielding a high surface area of 58 m^2/g and a density of 2.9 g/cm^3 (**Figure 3.1C)**. TGA results confirmed grafting reactions were successful as both the NS-g-PCL and NS-g-LTI showed sharp decreases in percent mass loss compared to that of the ungrafted NS control (**Figure 3.1A).** The effect of grafting NS on the crystallinity and grain size was investigated by XRD and revealed no change in the crystalline structure after grafting LTI and PCL to the surface of NS particles (**Figure 3.1B**). Average crystallite grain size was determined from XRD patterns using the Scherrer equation and ranged from 23 nm for the ungrafted NS particles to 28 nm for NS-g-PCL, with an average grain size of 24 nm for the NS-g-LTI particles. NS-LTI prepolymer grafting kinetics revealed complete conversion of surface hydroxyl groups and the creation of a stable viscous solution. The kinetics of this reaction were modeled using 2^{nd} order kinetics discussed in Chapter 2, and a reaction rate of 0.00143 $L*mol^{-1}*hr^{-1}$ (0.0343 $L*mol^{-1}*days^{-1}$) was calculated (**Figure 3.1D-E**). This value is within the same order of magnitude as the value calculated for nHA purchased from Sigma in Chapter 2 (0.0159 $L*mol^{-1}*days^{-1}$), with the reaction rate slightly higher for the NS nHA particles. As expected, OH conversion reached near 100%, while NCO conversion leveled out near 15% (**Figure 3.1F-G**).

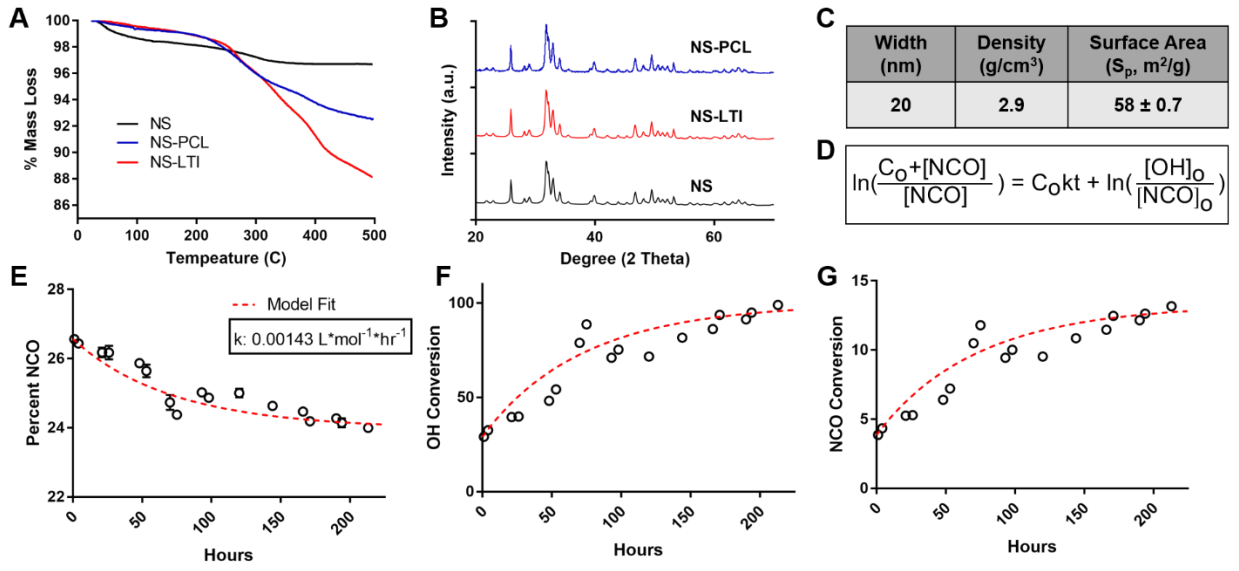

Figure 3.1: Characterization of NanoStim™ (NS) nHA grafted particles and prepolymer. (A) TGA summary of NS, NS-g-PCL, and NS-g-LTI show successful surface modification. (B) X-ray diffraction (XRD) patterns for NS, NS-g-PCL, and NS-g-LTI show no change in NS crystallinity (C) NS characterization, including particle width, density and surface area. (D) NS-LTI prepolymer 2nd order reaction kinetic model solution and (E) NS-LTI prepolymer grafting kinetics time course study at 40 °C with model fit overlay. (F) OH and (G) NCO conversion for NS-LTI grafting reaction with model fit.

nHA-TK, nHA-LTI, CaP, and sucrose were sterilized using radiation and composites fabricated under sterile conditions for cytotoxicity testing. Both the 0C0S and the 10C35S putty showed no signs of causing cell lysis or toxicity. The putties incorporated a total of 14 vol% nHA and nHA-PTKUR glue contained 25 vol%. This high HA content allowed for visualization of the nHA-PTKUR polymer using µCT. 2D µCT reconstructions of leached samples revealed minimal porosity for the 45C0S group and an increase in porosity with increasing sucrose, as anticipated (**Figure 3.2A**). SEM images paralleled these findings (**Figure 3.2B**).

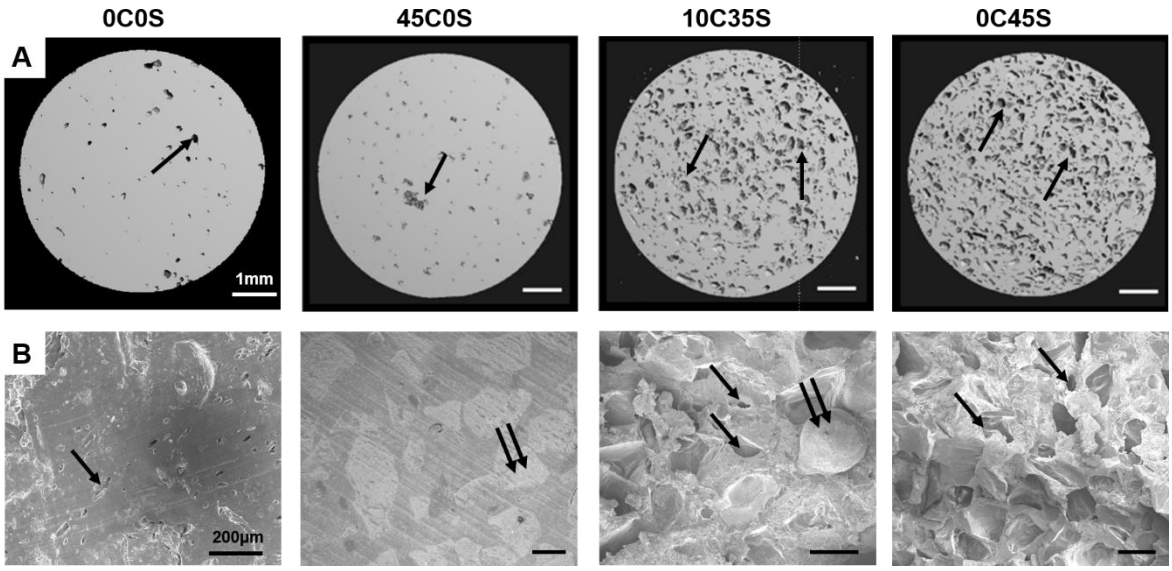

Figure 3.2: **Porosity characterization of NS-PTKUR bone cements**. (A) Images of 2D µCT cross-sections of 0C0S, 45C0S, 10C35S, 0C45S reveal the presence of pores (arrows). (B) SEM images of 0C0S, 45C0S, 10C35S, 0C45S show evidence of pores (single arrows) and ceramic granules (double arrow).

Mechanical Testing. All samples were leached in water for 5 days prior to mechanical testing. nHA-PTKUR glue (0C0S) exhibited a significantly higher ultimate strength, yield strength, and yield strain than any of the putties. The addition of sucrose porogens (10C35S, 0C45S) did not have a significant effect on ultimate strength, yield strength or yield strength over that of the CaP loaded putty group (45C0S) (**Figure 3.3B-D**). The moduli of the 0C0S and 45C0S putty were similar (370 MPa), but there was a significant difference between the modulus of the 45C0S putty and the 10C35S putty that incorporated porogen (**Figure 3.3A**).

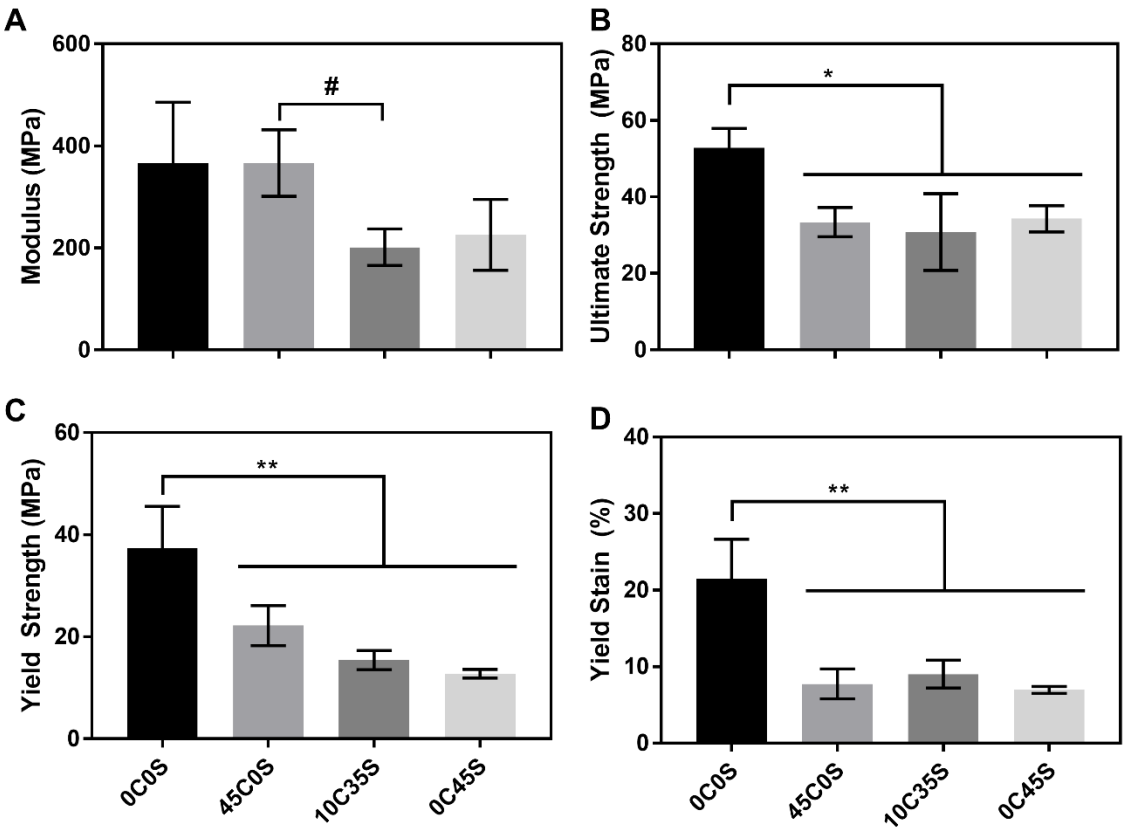

Figure 3.3: **Mechanical properties of NS-PTKUR bone cements**. (A) Young's modulus, (B) ultimate strength, (C) yield strength, and (D) yield strain measured under quasi-static compressive loading. The modulus of 45C0S was significantly higher than that of 10C35S. The ultimate strength, yield strength, and yield strain of 0C0S were significantly higher compared to any of the other groups. (#: $P \leq 0.1$, *: $P \leq 0.05$, **: $P \leq 0.01$).

In vivo analysis of nHA-PTKUR in rabbit hind-limb defects. Remodeling of nHA-PTKUR implants with four different solid and porogen loading ratios were investigated in femoral condyle plug defects in rabbits. µCT analysis revealed a statistically significant decrease in defect length from 4 to 18 months in all groups and all groups trended shorter for each timepoint, but large variation in defect width made it challenging to characterize changes in defect diameter (**Figure 3.4C-D**). BV/TV analysis revealed temporal and spatial changes in bone volume (**Figure 3.4E-H**).

A constant threshold that included bone but eliminated nHA-PTKUR and CaP particles was maintained for all groups at all time points (**Figure 3.4B**). However, the high radiodensity of CaP particles caused the surrounding nHA-PTKUR to appear denser than in other groups and consequently an increasing BV/TV as the core of the defect was approached was observed (**Figure 3.4F**). Therefore, BV/TV could only be compared within each material group. Changes in BV/TV as revealed by µCT were negligible in most cases with the most changes occurring in Pipe 1, at the outer perimeter of the defect. The 10C35S group trended as anticipated with a slightly higher BV/TV at each time point for all pipes (**Figure 3.4G**).

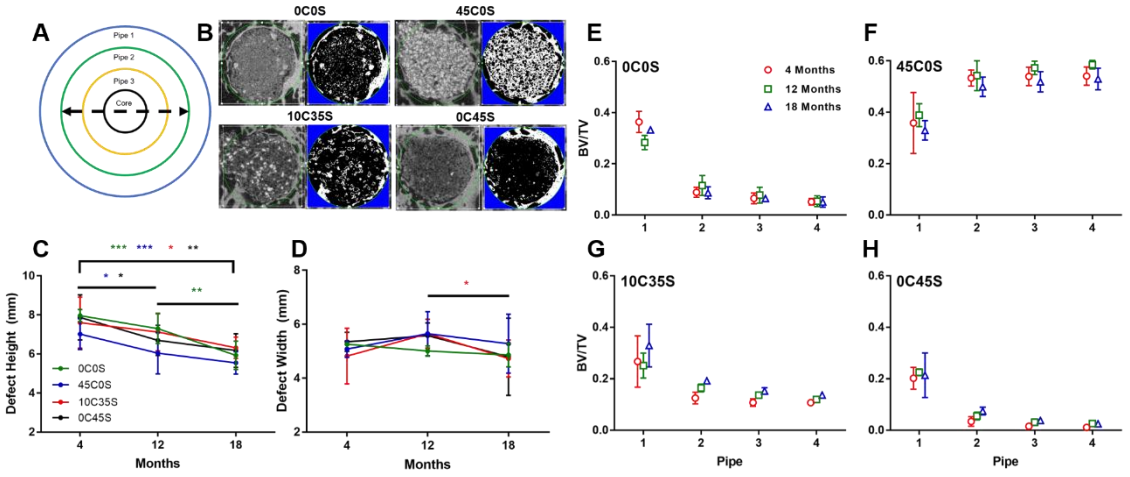

Figure 3.4: Analysis of bone healing by micro-computed tomography (µCT**).** (A) A schematic representation of the BV/TV µCT analysis procedure demonstrates the selection of concentric annular cylinders represented by the colored pipes. The dotted line and outer edge of the green circle represent the defect diameter. (B) Sample 2D images show the effects of thresholding on each of the different material groups. (C-D) 2D µCT reconstructions were used to measure the (C) length and (D) diameter of the defects at 4, 12, and 18 months. (E-H) The results of the BV/TV analysis are presented for the (E) 0C0S, (F) 45C0S, (G) 10C35S, and (H) 0C45S groups. (*: $P \leq 0.05$, **: $P \leq 0.01$, ***: $P \leq 0.001$).

New bone, cellular activity, and material degradation can be distinguished using Stevenel's Blue histological stain. A combination of endochondral and intramembranous ossification was

evident for all groups at 4, 12 and 18 months. The 0C0S demonstrated significant cellular infiltrate at the periphery of the graft at four months (**Figure 3.5A**). New bone (*) was evident within the graft space, multi-nucleated osteoclast-like cells (double arrow) were seen at the interface of the samples, and bone-forming cells were depositing osteoid (single arrow) at the interfaces of new bone and nHA-PTKUR. Cartilage-like, dark nodules were abundant near the perimeter of the graft (#) and cartilage mineralization was ongoing. A similar response is evident at 12 and 18 months and cartilage mineralization progressed. Polymer degradation was notably slower for the 0C0S group. The 45C0S group had less cellular infiltration at 4 months than other groups (**Figure 3.5B**), but a greater response of macrophages and giant cells was evident at the graft perimeter. At later time points cellular infiltration progressed, but compared to other groups, polymer resorption was stagnant at 12 and 18 months. Cartilage nodules were dispersed throughout the polymer towards the center of the graft and cartilage mineralization was ongoing at 12 and 18 months. The 10C35S group demonstrated new bone, endochondral bone formation, and intramembranous bone formation at four months (**Figure 3.5C**), and a similar combination of bone formation was seen closer to the center of the graft at 12 and 18 months. By 18 months new bone formation within the center of the graft was apparent and cellular infiltration was significant with osteoclast-like, giant cells present. The response to the 0C45S group was similar to the 10C35S group with new bone evident further within the implant at all time points (**Figure 3.5D**). At later time points, 0C45S showed evidence of significant scaffold degradation with the presence of osteoclast-like cells deep within the graft.

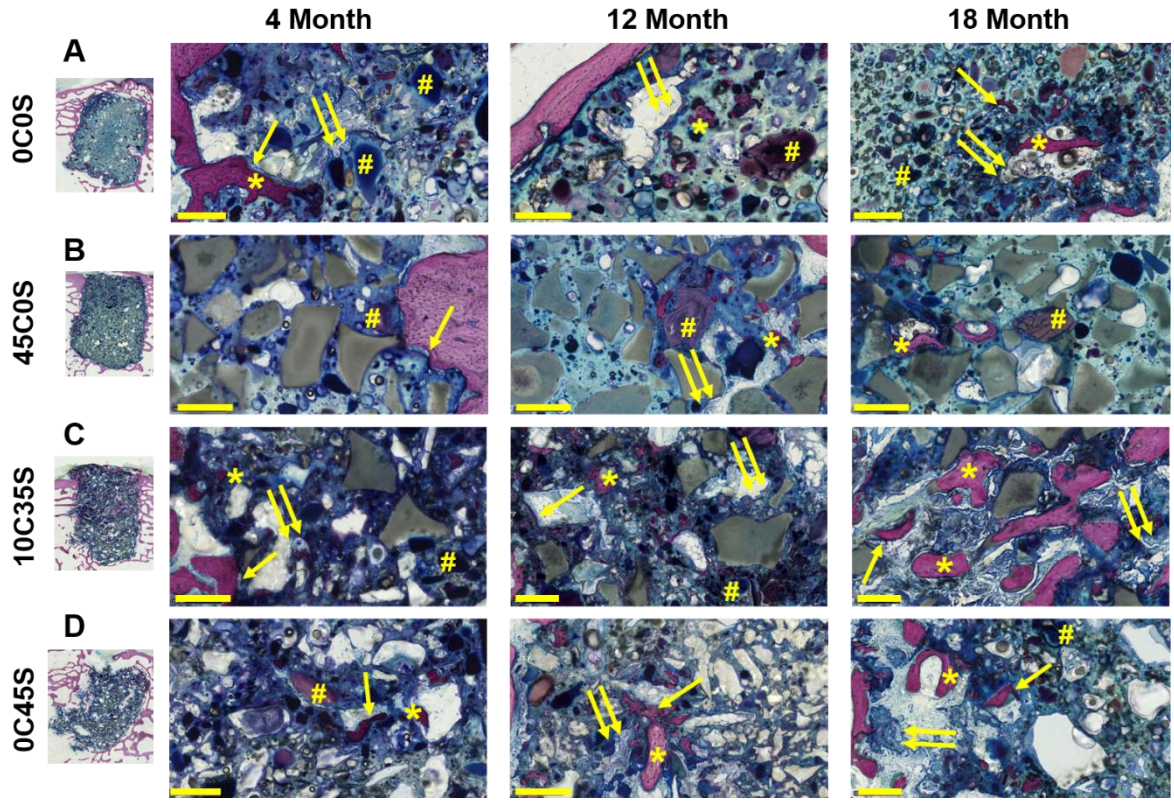

Figure 3.5: Histological characterization of NS-PTKUR bone cements. Magnified histology images of the (A) 0C0S, (B) 45C0S, (C) 10C35S, and (D) 0C45S groups at 4, 12 and 18 months stained with Stevenel's Blue demonstrate a combination of endochondral bone formation, indicated by the presence of cartilage-like nodules (#), and intramembranous bone formation, indicated by bone formation (single arrows) and osteoclast-like cells (double arrows) at the PTKUR interface. New bone (*) is evident within the PTKUR bone grafts at 4, 12 and 18 months. (scale bar = 250 µm, *: new bone, #: cartilage-like nodules, single arrow: bone lining cells and osteoid, double arrows: osteoclast-like cells).

Positive staining of Safranin O/Fast green verified the presence of cartilage nodules within the grafts (pink stain, single arrow) and better demonstrated mineralization of cartilage to bone (teal stain, double arrow) (**Figure 3.6**). Each group revealed presence of cartilage staining throughout the graft, with positive staining found deep within the tissue graft. The 0C0S demonstrated positive cartilage staining primarily near the periphery of the graft at all time points with greater positive staining deeper into the scaffold at later time points (**Figure 3.6A**). Each time point revealed ongoing cartilage mineralization. The 45C0S group demonstrated a similar response

to the 0C0S group with positive cartilage staining seen at all time points (**Figure 3.6B**). Ongoing cartilage mineralization was apparent at 4, 12 and 18 months, and relative to the 0C0S group, high amounts of ongoing cartilage mineralization were apparent near the center of the defect especially at 18 months. The 10C35S stained for positive cartilage nodules and cartilage mineralization at all time points. As early as 4 months cartilage nodules were seen, and ongoing mineralization was highly expressed at 12 months and interestingly lesser activity visualized at 18 months (**Figure 3.6C**). The 0C45S revealed the greatest positive staining for both cartilage nodules and cartilage mineralization to bone at early and late time points. At 4 months, especially at the center of the defect, high amounts of cartilage nodule staining were seen, but by 12 and 18 months the number of cartilage nodules decrease relative to the 4 month staining (**Figure 3.6D**). Overall, every group trended toward higher cartilage staining (pink/red stain) near the center of the defect and decreased slightly towards the periphery of the defect suggesting ongoing endochondral bone formation occurring deep within the scaffold.

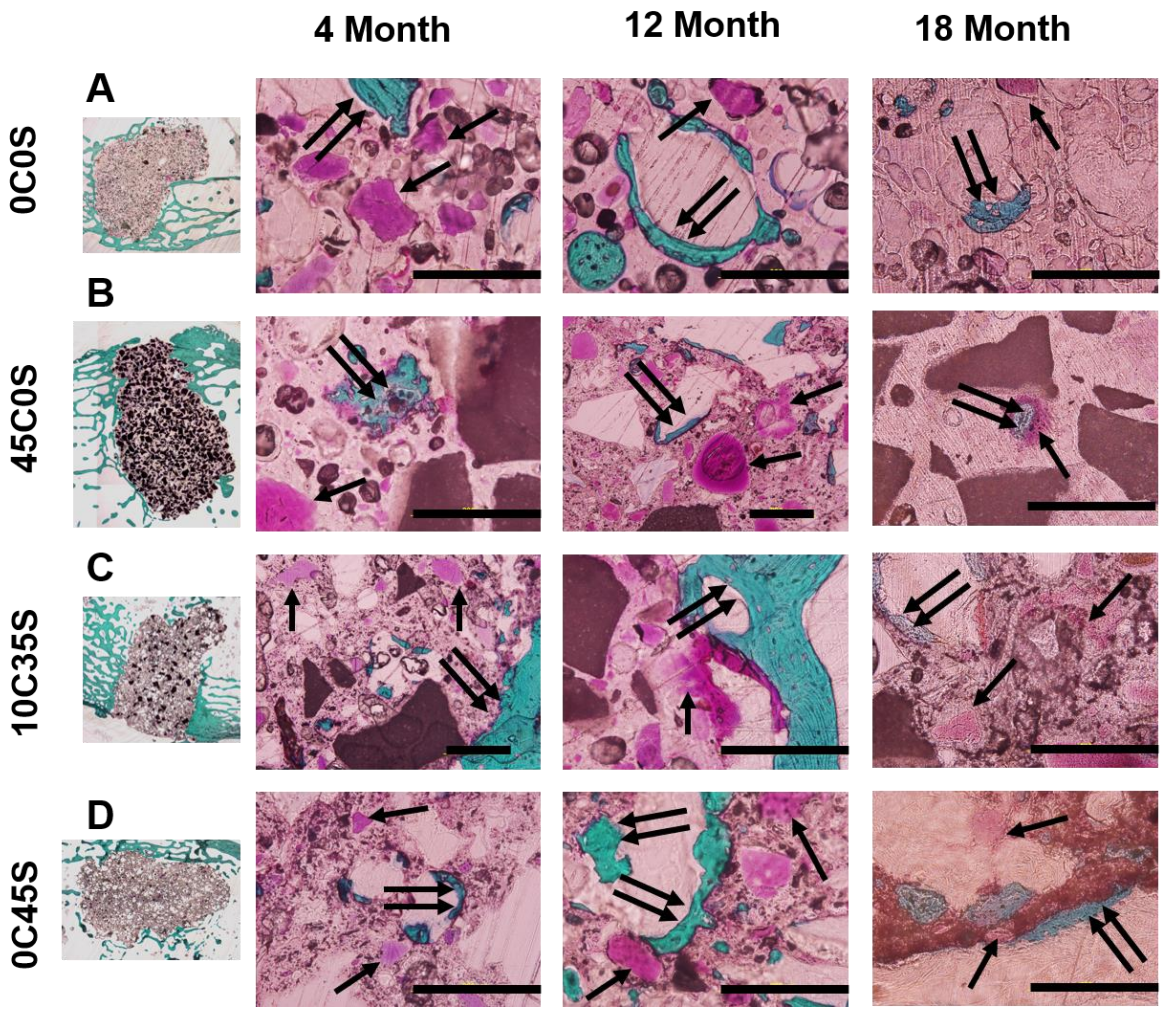

Figure 3.6: Safranin O histological characterization of NS-PTKUR bone cements. Histology images of the (A) 0C0S, (B) 45C0S, (C) 10C35S, and (D) 0C45S groups at 4, 12 and 18 months sections stained with Safranin O/Fast green. Collagen (pink stain, single arrows) was evident within the scaffold as early as 4 months and continued at all time points in every group. Bone (teal, double arrows) was also easily distinguished using this stain. (Scale bar: 200 µm).

Histomorphometry was performed on the distal half of the defects to quantify differences in bone (**Figure 3.7A**), cartilage-like dark nodules (**Figure 3.7B**), and porosity within the scaffold (**Figure 3.7C**). In all groups percent bone trended down as the center of the graft was approached, as expected, and only small changes were evident from 4 to 18 months. The sucrose group (0C45S) demonstrated the most change from 4 to 18 months in region three, at the host-bone/defect

interface, and region two which indicates bone ingrowth (**Figure 3.7A)**. Histomorphometry plots show an upward trend for bone ingrowth over time for all groups, and especially for the groups containing sucrose (10C35S, 0C45S). For the 0C0S glue group, very little bone tissue was observed in the central region (1), while greater amount of bone ingrowth was seen near the bone/defect interface at all time points (region 3). Dark-stained cartilage nodules were evident in all groups, and typical deep within the graft in region one to two (**Figure 3.7B**). Fewer cartilage-nodules were evident in the 0C0S group compared to other groups, especially in the center of the scaffold. Cartilage-nodules staining spiked in region three of the 0C0S group near the periphery, and very low cartilage staining was evident for the 45C0S group. The highest staining was seen in the central region (1) of the groups containing sucrose (0C45S) and in all regions at the 4-month time point. Interestingly at 12 months, the CaP/Sucrose group (10C35S) showed the highest staining for cartilage-like nodules. By 18 months, the 45C0S showed the highest staining at the center of the defect (1) with the two sucrose loaded groups (10C35S, 0C45S) showing notably lower cartilage-nodule staining. As expected, groups with sucrose additive (10C35S, 0C45S) trended towards higher porosity at all time points, especially towards the center of the grafts (**Figure 3.7C**). Interestingly at 4 months, the 0C0S and 45C0S showed similar porosity at the center region (1) to groups loaded with sucrose additive. Yet, at later times points (12 and 18 month) porosity for these groups (0C0S and 45C0S) decreased in region one. Generally, porosity increased for all groups when moving out from the center of the graft.

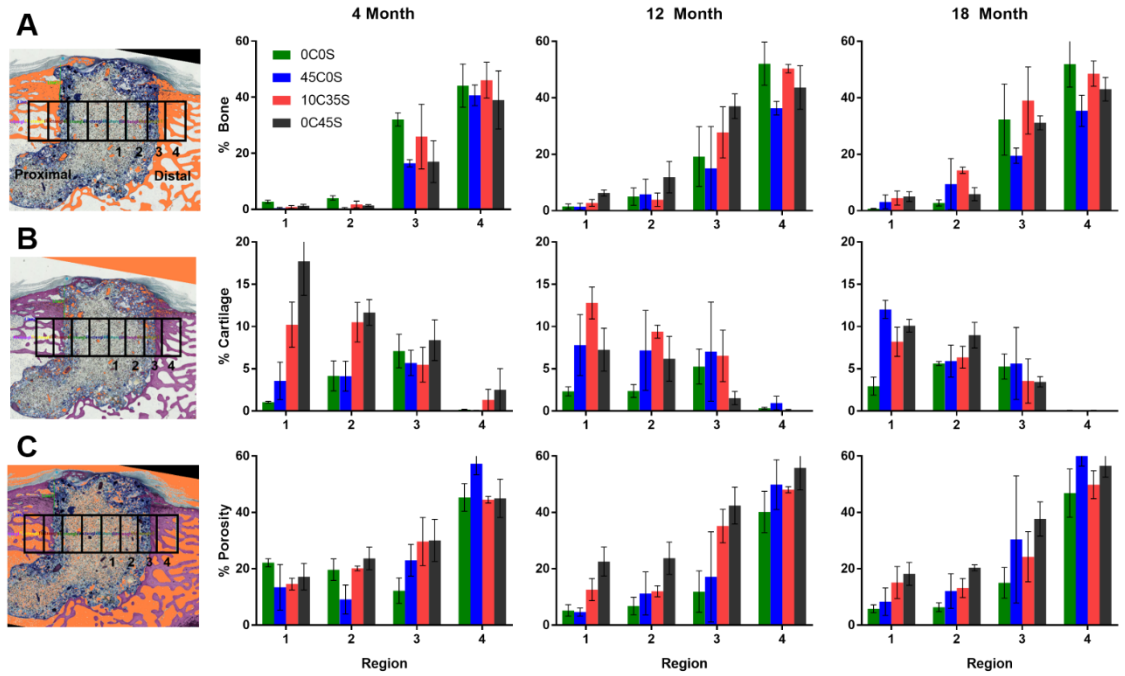

Figure 3.7: Histomorphometric analysis of new bone and cartilage formation in NS-PTKUR bone cements. Histomorphometric analysis of (A) area% bone, (B) area% cartilage (C) area% porosity in Stevenel's Blue stain for 0C0S, 45C0S, 10C35S and 0C45S at 4, 12 and 18 months. Thresholding can be visualized as orange coloring in images for each group.

An updated immunohistochemistry staining for ground sections was performed in 18-month PTKUR grafts to assess the presence of collagen 10 markers either within the center of the graft or near the edges. This testing was performed to further confirm the hypothesis that these PTKUR bone grafts were undergoing endochondral ossification remodeling in parallel to the classical intramembranous ossification typically seen in scaffold remodeling.[36] In the CaP loaded putty (45C0S) group, positive collagen 10 staining (pink/red, single arrow) was seen deep with the scaffold and near the edges (**Figure 3.8**). This suggests the presence of chondrocytes and chondrogenesis occurring with these scaffolds and more specifically the presence of hypertrophic chondrocytes typically seen in hypoxic environments.[37]

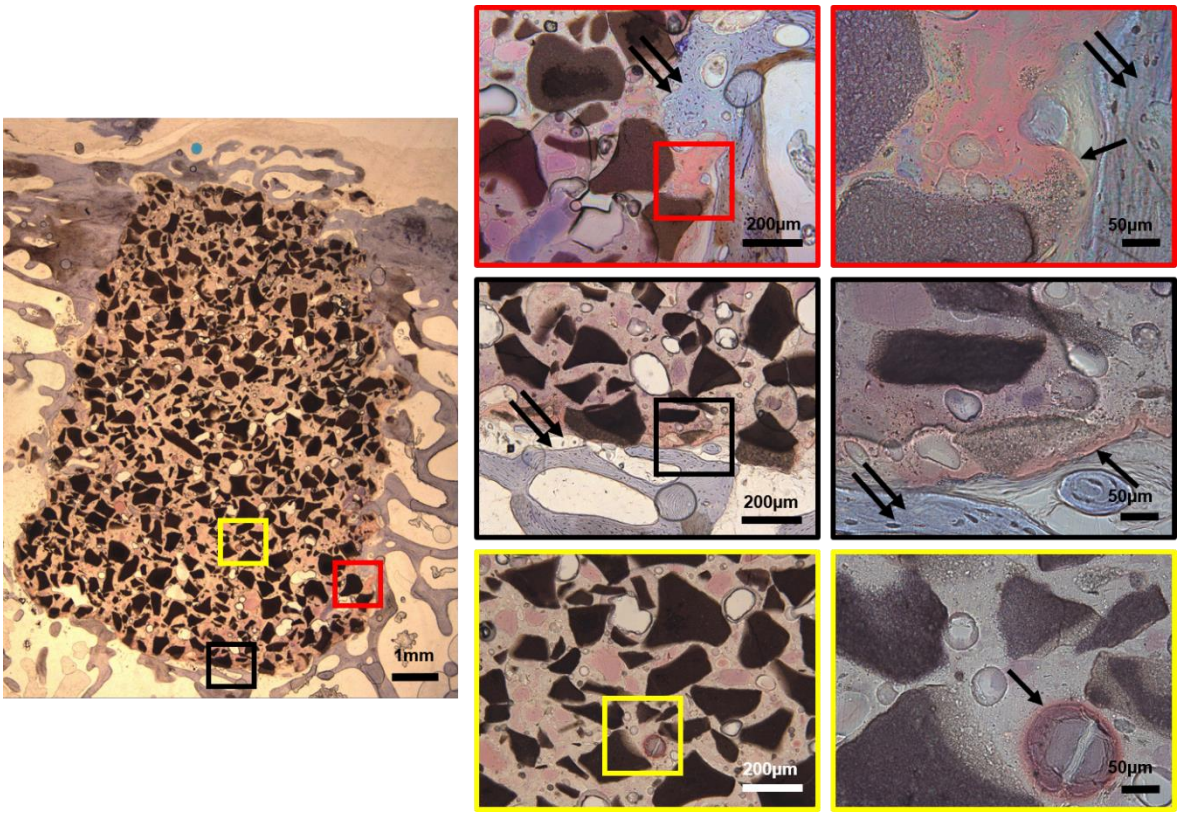

Figure 3.8: Immunohistochemistry staining for collagen 10 in NS-PTKUR bone cements. Positive collagen 10 immunohistochemistry (IHC) staining in 18-month, CaP loaded PTKUR defect (45C0S) in the center and surrounding edges of graft. Collagen 10 positive staining pink/red (single arrow) and bone blue/turquoise (double arrow).

Tibial slot defects were created to investigate remodeling in non-critical defects and the potential for the nHA-PTKUR to act as a "bone glue". Axial sections from the center of the tibial defects were stained with Stevenel's Blue. Islands of new bone were evident as early as four months. These islands were more abundant and more infiltrated at 12 and 18 months (**Figure 3.9A**). The experimental group exhibited significant ingrowth of new bone from the defect edges at 12 and 18 months and the perimeter of new bone was close to bridging at the nHA-PTKUR edges. Dark-stained cartilage-nodules seen in grafts in the femoral condyle were also present in the tibial slots. Unfilled tibial slot defects bridged by the four-month time period and dense, cortical-like bone was replaced by trabecular bone by 12 months (**Figure 3.9B**).

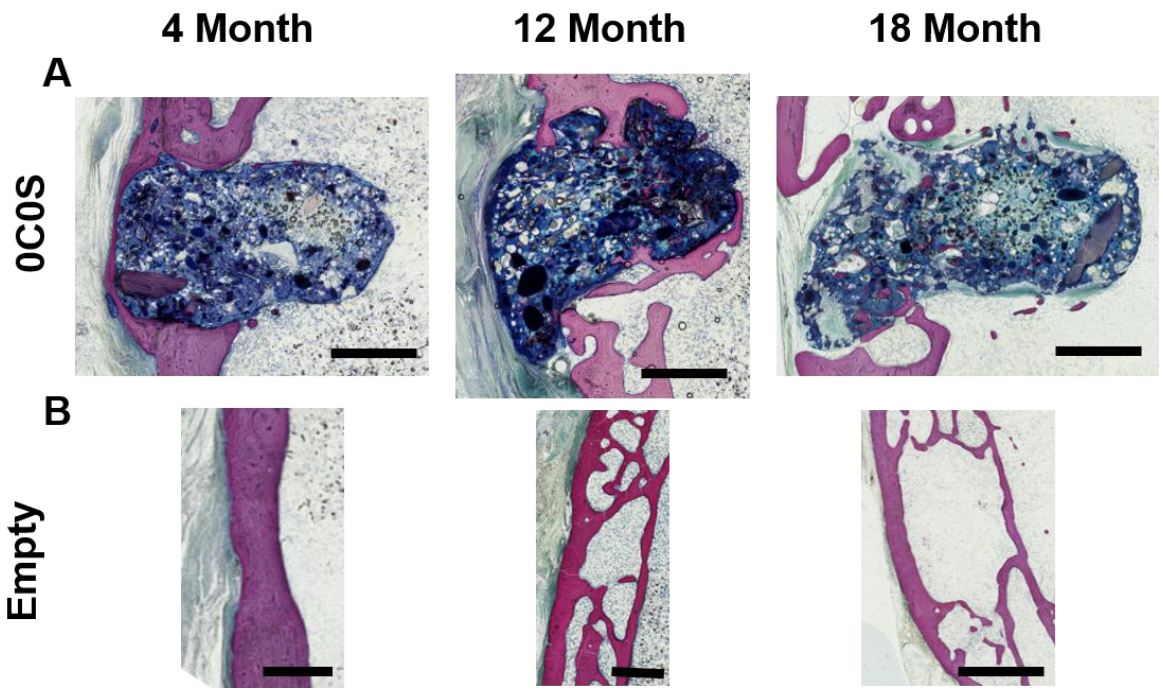

Figure 3.9: Histological characterization in tibial slot defect of PTKUR bone cement. Axial histology images of tibial slot defects demonstrate the (A) PTKUR glue (0C0S) persisted in the defect at 4, 12 and 18 months, and (B) empty tibial slots remodeling by 4 months. (Scale bar: 1mm)

3.5 Discussion

In this study, a nHA-PTKUR material that incorporated 20 nm nHA in both phases of the PUR precursor materials was developed. By adding 50 wt% nHA in the TK diol phase and 40 wt% nHA in the nHA-LTI prepolymer, favorable handling properties were achieved. The similar phases are anticipated to improve mixing and minimize phase separation for maximum mechanical properties.[6] Previous work incorporated 65 wt% nHA in an nHA-LTI prepolymer; however, this method necessitated the addition of catalyst to maintain flowability and a reactive prepolymer may decrease storage time.[19, 25] Furthermore, FeAA catalyst was included in the TK phase which decreased fabrication steps necessary in the surgical suite and eliminated the ε-caprolactone catalyst carrier used previously.[12] An NCO:OH index of 120 yielded similar volumes of each phase for potential delivery of an nHA-PTKUR glue (0C0S group) through a 1:1 double barrel syringe.

The short fiber shape of the NS nHA compared to the spherical shape of nHA used previously (19.5 m^2/g, 100 nm) led to an increase in nHA surface area of 38.5 m^2/g.[19] This smaller grain size is anticipated to enhance cellular attachment and new bone formation. Also, higher NS surface area is expected to enhance reactivity and interfacial bonding of the OH groups of nHA with the NCO reactive groups on LTI.[19, 28, 38-42]

Enhanced interfacial bonding was anticipated to increase mechanical properties of the nHA-PUR composite and allow for the addition of porosity without sacrificing bone-like strength.[38] Previously, a hybrid polymer composed of nHA-LTI and polycaprolactone triol (MW=300 g/mol) demonstrated mechanical properties sufficient for weight-bearing applications.[19, 25] The mechanical properties for the nHA-PTKUR material were a factor lower since a diol is anticipated to exhibit a lower crosslink density than the triol. In another study, PTKUR blended with 60 wt% ungrafted nHA demonstrated a maximum modulus of 1300 MPa and yield strength of 90 MPa after 1 week cure in ambient conditions.[12] PTKUR without nHA and 55 wt% CaP had a modulus of 940 MPa and yield strength of 40 MPa after 1 week. The significantly higher mechanical properties are attributed to higher nHA volume (compared to 45 wt% in the current study) and a higher wt% CaP (compared to 45 wt% in the current study). Additionally, nHA-PTKUR nanocomposite materials were left in ambient temperatures only 24 hours prior to leaching. The mechanical properties of the nHA-PTKUR nanocomposites are comparable to the mechanical properties reported 24 hours post-cure in the previous study.[12] Furthermore, nHA-PTKUR nanocomposites (including the 0C0S and 45C0S materials) were immersed in water for five days prior to mechanical testing for consistency between the sucrose containing materials and non-sucrose containing nHA-PTKURs. All groups demonstrated mechanical properties exceeding those of trabecular bone (compressive strength: 5-10 MPa,

modulus: 50-400 MPa).[43] Subjecting the nHA-PTKUR to a physiologically relevant environment and cure time (ie. cure time to match non-weight-bearing recovery time) may provide better insight to the potential for weight-bearing applications (strength = 70-90 MPa).[44]

nHA-PTKUR alone (0C0S), and putties materials containing 45 wt% CaP particles (45C0S), 35 wt% CaP and 10 wt% sucrose (10C35S), or 45 wt% sucrose (0C45S) were implanted in femoral condyle cylindrical defects bilaterally in rabbits. The nHA-PTKUR materials exhibited extensive cellular infiltration and osteogenesis at 4, 12 and 18 months. All groups demonstrated a combination of intramembranous and endochondral bone formation. Intramembranous bone formation describes the direct differentiation of MSCs to osteoblasts and the subsequent deposition of bone.[45, 46] During endochondral bone formation, MSCs proceed down the chondrogenic pathway and the cartilaginous callus is remodeled to bone.[45, 47] Stevenel's Blue staining revealed the presence of irregularly shaped nodules embedded within the nHA-PTKUR. Safranin O/Fast green staining methods were adapted for ground sections to verify these nodules were cartilaginous in nature and revealed mineralization of some of the nodules was ongoing. Dennis, et al. promote tissue engineering strategies that harness endochondral ossification, suggesting that following the principles of developmental skeletogenesis may enhance bone regeneration.[48] Still others believe these processes cannot occur simultaneously as primarily direct intramembranous formation in cancellous healing occurs with typically little cartilage seen.[49]

A PUR/allograft biocomposite in a critical size rabbit calvarium exhibited both intramembranous and endochondral bone formation; however, chondrogenesis was prevalent in large voids away from the implanted material, so the PUR did not likely influence this mechanism.[4] The combination of mechanisms demonstrated in the present study is hypothesized to be a result of the minimal porosity of the nHA-PTKUR and the concentration of nHA embedded in the PUR

structure.[19] Chondrogenesis thrives in hypoxic conditions anticipated where porosity is low, and osteogenesis is more likely to occur in oxygenated environments.[48, 50] Interestingly, literature also points to the development of hypoxic zones caused by the mineralization process and suggests that hypoxic conditions may favor osteocytogenesis.[51] Positive IHC staining for collagen 10 found in 18 month defects works to confirm this hypothesis as collagen 10 is a positive marker for hypertrophic chondrocytes typically seen in the transitional regions of chondrogenesis in hypoxic environments.[37, 50] These findings and the current work suggest the impact of oxygen content on bone graft remodeling mechanisms. To further confirm the presence collagen 10, as well as other chondrocyte makers, these PTKURs should be stained in cryo or paraffin sections, as the methods for IHC in ground sections can lead to non-specific binding.

Stevenel's Blue staining also revealed differential staining of the nHA-PTKUR. This was most evident in the minimally porous glue specimen where the polymer stained darker blue at the perimeter and lighter towards the core of the implant. The darker blue was higher towards the core of the implant for the material groups that incorporated porogen. Dark blue staining was evident in the glue implanted in the tibial defect, especially along the plane of host-bone after four months and a majority of the graft was stained dark blue after 12 and 18 months. Previous investigations of polypropylene meshes showed a similar phenomenon and the authors proved preferential histological stain uptake in microcracks within the material formed as a result of degradation.[52] Given the patterns of dark blue staining of the four groups included in the present work, alterations in the nHA-PTKUR are likely the cause of the enhanced staining.

Defect length measured from 2D μCT reconstructions taken from the center of the defect indicated material incorporation and new bone formation at 4, 12, and 18 months. Some material was forced out of the defect space and into the marrow space proximal to the condyles during

implantation causing large variation in defect width measurements. The Area of Interest (AOI) for histomorphometry was chosen to be similar to the Volume of Interest (VOI) used in μCT analysis. The regions for histomorphometry were slightly larger than for μCT analysis but normalizing to the size of the AOI (ie. bone percent) should allow for comparison. Histomorphometry demonstrated a higher percent bone for all regions compared to μCT. nHA-PUR polymers require stringent μCT thresholding given the mineral content of the polymer (and CaP), so a smaller scan voxel size may minimize the discrepancy between the two modes of measurement. Furthermore, the VOI for μCT included the proximal volume where graft may have overflowed into the marrow space during implantation. This added graft material outside of the defined defect space will have a lower percent bone than if the defect space was appropriately surrounded by trabecular bone.

3.6 Conclusion

This work describes the formulation of an injectable, settable, and cell-degradable nHA-PTKUR bone void filler that incorporated up to 25 vol% nHA. The addition of CaP particles and/or sucrose improved handling properties for a moldable putty and sucrose leaching induced porosity without sacrificing bone-like mechanical properties. Both the nHA-PTKUR glue and the putties demonstrated controlled remodeling via a unique combination of intramembranous and endochondral bone formation at 4, 12 and 18 months when implanted in the femoral condyles of rabbits. Furthermore, the remodeling rate can be altered for the desired application by adjusting the CaP:sucrose ratio. These findings show that the addition of nHA to a PTKUR enhances bone cell activity. Furthermore, implantation of four variations of nHA-PTKUR bone grafts in two preclinical models demonstrates the potential of nHA-PTKUR as injectable and moldable tissue engineering bone grafts that can be tuned for the desired implantation methods and remodeling demands of various applications.

3.7 References

1. Adhikari, R.; Gunatillake, P. A.; Griffiths, I.; Tatai, L.; Wickramaratna, M.; Houshyar, S.; Moore, T.; Mayadunne, R. T.; Field, J.; McGee, M.; Carbon, T., Biodegradable injectable polyurethanes: synthesis and evaluation for orthopaedic applications. *Biomaterials* **2008,** *29* (28), 3762-3770.
2. Adolph, E. J.; Guo, R.; Pollins, A. C.; Zienkiewicz, K.; Cardwell, N.; Davidson, J. M.; Guelcher, S. A.; Nanney, L. B., Injected biodegradable polyurethane scaffolds support tissue infiltration and delay wound contraction in a porcine excisional model. *Journal of Biomedical Materials Research Part B: Applied Biomaterials* **2015**.
3. Bonzani, I. C.; Adhikari, R.; Houshyar, S.; Mayadunne, R.; Gunatillake, P.; Stevens, M. M., Synthesis of two-component injectable polyurethanes for bone tissue engineering. *Biomaterials* **2007,** *28* (3), 423-433.
4. Dumas, J. E.; BrownBaer, P. B.; Prieto, E. M.; Guda, T.; Hale, R. G.; Wenke, J. C.; Guelcher, S. A., Injectable reactive biocomposites for bone healing in critical-size rabbit calvarial defects. *Biomedical Materials* **2012,** *7* (2), 024112.
5. Guelcher, S. A.; Patel, V.; Gallagher, K. M.; Connolly, S.; Didier, J. E.; Doctor, J. S.; Hollinger, J. O., Synthesis and In Vitro Biocompatibility of Injectable Polyurethane Foam Scaffolds. *Tissue Engineering* **2006,** *12* (5), 1247-59.
6. Guelcher, S. A.; Srinivasan, A.; Dumas, J. E.; Didier, J. E.; McBride, S.; Hollinger, J. O., Synthesis, mechanical properties, biocompatibility, and biodegradation of polyurethane networks from lysine polyisocyanates. *Biomaterials* **2008,** *29* (12), 1762-1775.
7. Hafeman, A. E.; Zienkiewicz, K. J.; Zachman, A. L.; Sung, H.-J.; Nanney, L. B.; Davidson, J. M.; Guelcher, S. A., Characterization of the degradation mechanisms of lysine-derived aliphatic poly(ester urethane) scaffolds. *Biomaterials* **2011,** *32* (2), 419-429.
8. Nagata, M.; Oi, A.; Sakai, W.; Tsutsumi, N., Synthesis and properties of biodegradable network poly (ether-urethane) s from L-lysine triisocyanate and poly (alkylene glycol) s. *Journal of Applied Polymer Science* **2012,** *126* (S2).
9. Storey, R. F.; Wiggins, J. S.; Puckett, A., Hydrolyzable poly (ester-urethane) networks from l-lysine diisocyanate and d, l-lactide/ϵ-caprolactone homo-and copolyester triols. *Journal of Polymer Science Part A: Polymer Chemistry* **1994,** *32* (12), 2345-2363.
10. Dumas, J. E.; Davis, T.; Holt, G. E.; Yoshii, T.; Perrien, D. S.; Nyman, J. S.; Boyce, T.; Guelcher, S. A., Synthesis, characterization, and remodeling of weight-bearing allograft bone/polyurethane composites in the rabbit. *Acta Biomaterialia* **2010,** *6* (7), 2394-2406.
11. Dumas, J. E.; Prieto, E. M.; Zienkiewicz, K. J.; Guda, T.; Wenke, J. C.; Bible, J.; Holt, G. E.; Guelcher, S. A., Balancing the Rates of New Bone Formation and Polymer Degradation Enhances Healing of Weight-Bearing Allograft/Polyurethane Composites in Rabbit Femoral Defects. *Tissue Engineering Part A* **2014,** *20* (1-2), 115-129.
12. McEnery, M. A.; Lu, S.; Gupta, M. K.; Zienkiewicz, K. J.; Wenke, J. C.; Kalpakci, K. N.; Shimko, D. A.; Duvall, C. L.; Guelcher, S. A., Oxidatively degradable poly (thioketal urethane)/ceramic composite bone cements with bone-like strength. *RSC advances* **2016,** *6* (111), 109414-109424.
13. Cisneros-Pineda, O. G.; Herrera Kao, W.; Loría-Bastarrachea, M. I.; Veranes-Pantoja, Y.; Cauich-Rodríguez, J. V.; Cervantes-Uc, J. M., Towards optimization of the silanization process of hydroxyapatite for its use in bone cement formulations. *Materials Science and Engineering: C* **2014,** *40* (0), 157-163.

14. Guda, T.; Walker, J. A.; Pollot, B. E.; Appleford, M. R.; Oh, S.; Ong, J. L.; Wenke, J. C., In vivo performance of bilayer hydroxyapatite scaffolds for bone tissue regeneration in the rabbit radius. *Journal of Materials Science: Materials in Medicine* **2011,** *22* (3), 647-656.
15. Guda, T.; Walker, J. A.; Singleton, B. M.; Hernandez, J. W.; Son, J.-S.; Kim, S.-G.; Oh, D. S.; Appleford, M. R.; Ong, J. L.; Wenke, J. C., Guided bone regeneration in long-bone defects with a structural hydroxyapatite graft and collagen membrane. *Tissue Engineering Part A* **2012,** *19* (17-18), 1879-1888.
16. Lee, J. H.; Hwang, C. J.; Song, B. W.; Koo, K. H.; Chang, B. S.; Lee, C. K., A prospective consecutive study of instrumented posterolateral lumbar fusion using synthetic hydroxyapatite (Bongros®-HA) as a bone graft extender. *Journal of Biomedical Materials Research Part A* **2009,** *90* (3), 804-810.
17. Lovati, A. B.; Lopa, S.; Recordati, C.; Talò, G.; Turrisi, C.; Bottagisio, M.; Losa, M.; Scanziani, E.; Moretti, M., In Vivo Bone Formation Within Engineered Hydroxyapatite Scaffolds in a Sheep Model. *Calcified Tissue International* **2016**, 1-15.
18. Clarke, B., Normal bone anatomy and physiology. *Clinical journal of the American Society of Nephrology* **2008,** *3* (Supplement 3), S131-S139.
19. Lu, S.; McGough, M.; Rogers, B.; Wenke, J.; Shimko, D.; Guelcher, S., Resorbable nanocomposites with bone-like strength and enhanced cellular activity. *Journal of Materials Chemistry B* **2017,** *5* (22), 4198-4206.
20. Mi, H. Y.; Palumbo, S.; Jing, X.; Turng, L. S.; Li, W. J.; Peng, X. F., Thermoplastic polyurethane/hydroxyapatite electrospun scaffolds for bone tissue engineering: effects of polymer properties and particle size. *Journal of Biomedical Materials Research Part B: Applied Biomaterials* **2014,** *102* (7), 1434-1444.
21. Mi, H.-Y.; Jing, X.; Salick, M. R.; Cordie, T. M.; Peng, X.-F.; Turng, L.-S., Morphology, mechanical properties, and mineralization of rigid thermoplastic polyurethane/hydroxyapatite scaffolds for bone tissue applications: effects of fabrication approaches and hydroxyapatite size. *Journal of Materials Science* **2014,** *49* (5), 2324-2337.
22. Tetteh, G.; Khan, A. S.; Delaine-Smith, R. M.; Reilly, G. C.; Rehman, I. U., Electrospun polyurethane/hydroxyapatite bioactive Scaffolds for bone tissue engineering: The role of solvent and hydroxyapatite particles. *Journal of the Mechanical Behavior of Biomedical Materials* **2014,** *39*, 95-110.
23. Yang, W.; Both, S. K.; Zuo, Y.; Birgani, Z. T.; Habibovic, P.; Li, Y.; Jansen, J. A.; Yang, F., Biological evaluation of porous aliphatic polyurethane/hydroxyapatite composite scaffolds for bone tissue engineering. *Journal of Biomedical Materials Research Part A* **2014**.
24. Cetina-Diaz, S. M.; Chan-Chan, L. H.; Vargas-Coronado, R. F.; Cervantes-Uc, J. M.; Quintana-Owen, P.; Paakinaho, K.; Kellomaki, M.; Di Silvio, L.; Deb, S.; Cauich-Rodriguez, J. V., Physicochemical characterization of segmented polyurethanes prepared with glutamine or ascorbic acid as chain extenders and their hydroxyapatite composites. *Journal of Materials Chemistry B* **2014,** *2* (14), 1966-1976.
25. Lu, S.; McGough, M. A.; Shiels, S. M.; Zienkiewicz, K. J.; Merkel, A. R.; Vanderburgh, J. P.; Nyman, J. S.; Sterling, J. A.; Tennent, D. J.; Wenke, J. C., Settable polymer/ceramic composite bone grafts stabilize weight-bearing tibial plateau slot defects and integrate with host bone in an ovine model. *Biomaterials* **2018**.
26. Xie, R.; Hu, J.; Ng, F.; Tan, L.; Qin, T.; Zhang, M.; Guo, X., High performance shape memory foams with isocyanate-modified hydroxyapatite nanoparticles for minimally invasive bone regeneration. *Ceramics International*.

27. Martin, J. R.; Gupta, M. K.; Page, J. M.; Yu, F.; Davidson, J. M.; Guelcher, S. A.; Duvall, C. L., A porous tissue engineering scaffold selectively degraded by cell-generated reactive oxygen species. *Biomaterials* **2014,** *35* (12), 3766-3776.
28. Webster, T. J.; Ergun, C.; Doremus, R. H.; Siegel, R. W.; Bizios, R., Enhanced functions of osteoblasts on nanophase ceramics. *Biomaterials* **2000,** *21* (17), 1803-1810.
29. MacMillan, A. K.; Lamberti, F. V.; Moulton, J. N.; Geilich, B. M.; Webster, T. J., Similar healthy osteoclast and osteoblast activity on nanocrystalline hydroxyapatite and nanoparticles of tri-calcium phosphate compared to natural bone. *International journal of nanomedicine* **2014,** *9*, 5627.
30. Standard, I., 9277,"Determination of the Specific Surface Area of Solids by Gas Adsorption Using the BET Method,". *International Organization for Standardization, Geneva, Switzerland* **1995**.
31. Harmata, A. J.; Ward, C. L.; Zienkiewicz, K. J.; Wenke, J. C.; Guelcher, S. A., Investigating the effects of surface-initiated polymerization of ε-caprolactone to bioactive glass particles on the mechanical properties of settable polymer/ceramic composites. *Journal of Materials Research* **2014,** *29* (20), 2398-2407.
32. Yubao, L.; De Groot, K.; De Wijn, J.; Klein, C.; Meer, S., Morphology and composition of nanograde calcium phosphate needle-like crystals formed by simple hydrothermal treatment. *Journal of materials science: Materials in Medicine* **1994,** *5* (6-7), 326-331.
33. International, A., Standard test method for isocyanate groups in urethane materials or prepolymers. ASTM International: 2010.
34. Harmata, A. J.; Uppuganti, S.; Granke, M.; Guelcher, S. A.; Nyman, J. S., Compressive fatigue and fracture toughness behavior of injectable, settable bone cements. *Journal of the mechanical behavior of biomedical materials* **2015,** *51*, 345-355.
35. International, A., ASTM F451-16, Standard specification for acrylic bone cement. West Conshohocken, PA, 2016.
36. Sun, M. M.; Beier, F., Chondrocyte hypertrophy in skeletal development, growth, and disease. *Birth Defects Res C Embryo Today* **2014,** *102* (1), 74-82.
37. Schipani, E., Hypoxia and HIF-1α in chondrogenesis. *Seminars in Cell & Developmental Biology* **2005,** *16* (4), 539-546.
38. Kickelbick, G., Concepts for the incorporation of inorganic building blocks into organic polymers on a nanoscale. *Progress in Polymer Science* **2003,** *28* (1), 83-114.
39. Laurencin, C. T.; Kumbar, S. G.; Nukavarapu, S. P., Nanotechnology and orthopedics: a personal perspective. *Wiley Interdisciplinary Reviews: Nanomedicine and Nanobiotechnology* **2009,** *1* (1), 6-10.
40. Liu, Q.; de Wijn, J. R.; de Groot, K.; van Blitterswijk, C. A., Surface modification of nano-apatite by grafting organic polymer. *Biomaterials* **1998,** *19* (11), 1067-1072.
41. Ngiam, M.; Liao, S.; Patil, A. J.; Cheng, Z.; Chan, C. K.; Ramakrishna, S., The fabrication of nano-hydroxyapatite on PLGA and PLGA/collagen nanofibrous composite scaffolds and their effects in osteoblastic behavior for bone tissue engineering. *Bone* **2009,** *45* (1), 4-16.
42. Sun, F.; Zhou, H.; Lee, J., Various preparation methods of highly porous hydroxyapatite/polymer nanoscale biocomposites for bone regeneration. *Acta Biomaterialia* **2011,** *7* (11), 3813-3828.
43. Fernando, S.; McEnery, M.; Guelcher, S., Polyurethanes for bone tissue engineering. *Advances in Polyurethane Biomaterials* **2016**, 481.

44. Kühn, K.-D., *Bone cements: up-to-date comparison of physical and chemical properties of commercial materials*. Springer 2000.
45. Gilbert, S., Osteogenesis: the development of bones. *Developmental biology* **2000,** *6*.
46. Stricker, S.; Mundlos, S., Chapter seven - FGF and ROR2 Receptor Tyrosine Kinase Signaling in Human Skeletal Development. In *Current Topics in Developmental Biology*, Birchmeier, C., Ed. Academic Press: 2011; Vol. 97, pp 179-206.
47. Akter, F.; Ibanez, J., Chapter 8 - Bone and Cartilage Tissue Engineering. In *Tissue Engineering Made Easy*, Academic Press: 2016; pp 77-97.
48. Dennis, S. C.; Berkland, C. J.; Bonewald, L. F.; Detamore, M. S., Endochondral Ossification for Enhancing Bone Regeneration: Converging Native Extracellular Matrix Biomaterials and Developmental Engineering In Vivo. *Tissue Engineering Part B: Reviews* **2014**.
49. Sandberg, O. H.; Aspenberg, P., Inter-trabecular bone formation: a specific mechanism for healing of cancellous bone. *Acta Orthop* **2016,** *87* (5), 459-465.
50. Bornes, T. D.; Jomha, N. M.; Mulet-Sierra, A.; Adesida, A. B., Hypoxic culture of bone marrow-derived mesenchymal stromal stem cells differentially enhances in vitro chondrogenesis within cell-seeded collagen and hyaluronic acid porous scaffolds. *Stem cell research & therapy* **2015,** *6* (1), 84.
51. Chen, X.; Wang, L.; Zhao, K.; Wang, H., Osteocytogenesis: Roles of Physicochemical Factors, Collagen Cleavage and Exogenous Molecules. *Tissue Engineering Part B: Reviews* **2018**.
52. Iakovlev, V. V.; Guelcher, S. A.; Bendavid, R., Degradation of polypropylene in vivo: A microscopic analysis of meshes explanted from patients. *Journal of Biomedical Materials Research Part B: Applied Biomaterials* **2015,** *105* (2), 237-248.

CHAPTER 4

CELL-DEGRADABLE THERMOPLASTIC POLY(THIOKETAL-URETHANE) ELASTOMERS FOR 3D PRITNING APPLCATIONS

4.1 Abstract

Fused deposition modeling (FDM) is a 3D printing technique in which thermoplastics are heated above their melting temperature, extruded, and deposited layer by layer to create 3-dimensional objects. FDM has emerged as a solution for biomedical devices as it represents a unique solution for creating detailed and variable devices in an additive manufacturing (AM) setting. Currently, biocompatible plastics capable of AM printing include materials such as polylactide (PLA) and poly(caprolactone) (PCL), which typically undergo hydrolytic degradation. However, non-specific degradation can result in a rapid clearance of polymer *in vivo* leading to an imbalance of cellular infiltration and scaffold degradation. Poly(thioketal urethanes) (PTKURs) represent a new family of chemistry for synthesis of degradable scaffolds for regenerative medicine. PTKUR scaffolds degrade by reactive oxygen species (ROS) secreted by cells as they infiltrate the scaffold. They are hydrolytically stable and will remain intact until cells-mediated degradation occurs. In this preliminary work, thermoplastic poly(thioketal urethane) (TPTKUR) elastomers are synthesized and their physical properties are characterized for future use with FDM. Thermal properties such as the glass transition temperature (T_g) and melting temperature (T_m) are determined as well as specific morphometric properties. The long-term goal is to further characterize and fabricate a TPTKUR biomedical implants with tunable properties for use in FDM, thus aligning the rate of tissue ingrowth with that of implant degradation.

4.2 Introduction

Fused deposition modeling (FDM) represents a new opportunity for additive manufacturing (AM) for a wide range of medical devices and implants.[1] Many biocompatible polymers have been developed that can be fabricated using FDM techniques which are resorbable such as polylactide (PLA), polycaprolactone (PCL) and others, but these polymers have been shown to undergo hydrolytic degradation.[2-5] To overcome the shortcomings of these polymers, a new family of poly(thioketals urethanes) (PTKURs) have been developed which are degradable by first order kinetics in the presence of cell-secreted reactive oxygen species (ROS) and are stable in hydrolytic environments.[6, 7]

In this work, we propose and evaluate the feasibility of developing a new class of thermoplastic-PTKURs (TPTKURs) elastomers which are capable of extrusion for use in FDM applications. Thermoplastic polyurethanes (TPURs) elastomers have been developed by others as biocompatible materials, but these conventional TPURs are non-resorbable.[8, 9] TPURs are synthesized by the combination of a large marcodiol soft segment with a hard segment consisting of a diisocyanate, with or without a chain extender, to create urethane linkage and a high molecular weight polymer. The elastomeric properties are derived due to thermodynamic incompatibilities between the hard and soft segments within the polymer framework[10, 11]. This phase immiscibility leads to unique morphological conditions known as microphase-separation which are primarily driven by hydrogen bonds forming within the hard segment carbonyl and amine bonds[11, 12]. The principles are governed by the Flory-Huggins parameter (χ^N) and increase as the difference between the solubility parameters of the hard and soft segments (δ_H - δ_S) increases.[10, 13, 14] Other groups have recently shown that hard segment symmetry plays a significant role in driving microphase-separation and influencing mechanical and thermal properties of their elastomers. [10,

[12, 15-17] It is hypothesized by Wilkes et al. that this is due to alignment and stacking of hard segments allowing greater hydrogen bonding to occur and the formation of a superior microphase-separated thermoplastic elastomer.[17]

We have leveraged these findings to create a microphase-separated TPTKUR elastomer with symmetric hard segments and cell-degradable PTK macrodiol soft segments. Microphase-separated TPURs exhibit a distinct glass-transition temperature (T_g) for the soft segment and a melting temperature (T_m) for the hard segment. An ideal biomaterial thermoplastic has a T_g well below room temperature (T_g < -40 ºC), and a T_m well above the service temperature (32 ºC), but at a reasonable range for FDM extrusion and deposition without affecting polymer stability (50 ºC < T_m < 200 ºC). Symmetric isocyanate hard segments have shown thermal properties in this range with poly(tetramethylene oxide) (PTMO) 1000 Da soft segments in prior studies.[11, 12] While these polymers microphase-separate, PTMO based TPURs are non-resorbable which limits their applications. Our new PTK macrodiols are cell-degradable and have similar solubility parameters to that of PTMO.[18] We hypothesize by replacing PTMO soft segments with PTK macrodiols, we can reproduce thermal properties while creating a degradable TPTKUR scaffold with degradation rates matching that of tissue ingrowth promoting regenerative tissue healing.[19]

In this preliminary study, a family of TPTKURs were synthesized and characterized by testing thermal and morphometric properties by DSC and FTIR respectively. Hexane diisocyanate (HDI) and cyclohexane diisocyanate (CHDI) were chosen as two symmetric hard segments for preliminary investigation, with or without chain extension with butane diol (BDO). 2-mercaptoethyl ether (MEE) and 2,2′-(ethylenedioxy) diethanethiol (EDDT) based PTK macrodiols (1000 – 1250 g/mol) were chosen as preliminary candidates to investigate the feasibility of creating a TPKUR segmented elastomer. MEE and EDDT macrodiols vary in hydrophilicity, which effects

the solubility parameters of each soft segment, and in turn will govern the extent to which the thermoplastic will microphase-separate.

4.3 Materials and Methods

Materials. All reagents for preliminary studies were purchased from Sigma (St Louis, MO), except for 2-bromoethanol and 2-mercaptoethyl ether (MEE which were purchased from Fischer. Hexane diisocyanate (HDI) was gifted from Covestro (Pittsburg, PA). All materials were used as received.

Poly(thioketal)hydroxyl-terminated synthesis. Synthesis was adapted from previously work done by Martin et al.[20] P-toluenesulphonic acid monohydrate (PTSA) was added to a three-neck round bottom flask with an addition funnel. Acetonitrile was charged to the vessel and batch-specific amounts of MEE or 2,2′-(ethylenedioxy) diethanethiol (EDDT) (x molar eq) were added. The addition funnel was charged with acetonitrile and 2,2-dimethoxypropane (DMP) (0.83 molar eq x). The temperature of the reaction was set to 80 ºC followed by the addition of DMP-acetonitrile dropwise into the continuously stirring boiling flask for 16 hours. The intermediate dithiol was recovered by rotary evaporation. To avoid disulfide bridging, immediate hydroxyl functionalization was performed. PTK dithiols were dissolved in tetrahydrofuran (THF) before adding a 5X molar excess of cesium carbonate ($CsCO_3$). The solution was stirred for 30 minutes at room temperature before adding a 4X molar excess of 2-bromoethanol stirred for 18 hours under inert atmosphere. The product was added to a separation funnel with excess water to effectively separate the PTK- solubilizing THF layer from the water-soluble $CsCO_3$ catalyst. The hydroxyl functionalized PTK was isolated from solvent by rotary evaporation and precipitated in cold ethanol. The product was thoroughly dried under vacuum and stored in a desiccator prior to use.

^{1}H NMR was utilized to verify structure and gel permeation chromatography (GPC) determined molecular weight.

Thermoplastic poly(thioketal urethane) synthesis. TPTKUR elastomer synthesis was adapted largely from work reported by Wilkes et al., and Pennings et al.[8-10, 21] Briefly, symmetric isocyanates either HDI or CHDI (1.03X mol eq.) were added to a 3-neck round bottom flask with dry dimethyl formamide (DMF) equipped with an addition funnel and condenser. PTKs (MEE or EDDT) (X mol eq.) were added to the addition funnel with additional DMF at 15 wt% solids and a single drop of dibutyltin dilaurate (DBTDL) catalyst. The flask was placed into an oil bath maintained at 80 ºC and PTK-DMF solution was added dropwise from addition funnel. After 21 hours, TPTKURs were precipitated directly from the reaction vessel into cold diethyl ether and separated using a Buchner funnel. Polymer was dried overnight at 40 ºC under vacuum.

For chain extended TPTKUR, similar reaction conditions were followed with a 2X mol eq. of HDI or CHDI to 1X mol eq. of PTKs at 18.5 wt% solids for 4 hours of reaction. Dried butane diol (BDO) chain extender (0.94X mol eq.) was then added with additional DMF at 15 wt% solids. The reaction continued for 21 hours followed by precipitation and a similar work up.

Thermoplastic poly(thioketal urethane) characterization. TPTKURs molecular weight was evaluated by GPC and thermal properties were assessed by differential scanning calorimetry (DSC). Morphometric evaluation was assessed by Fourier-transformed infrared spectrometry (FTIR). Thermal stability was assessed by thermogravimetric analysis (TGA) and degradation kinetics were determined using a 20% H_2O_2 /0.1 M $CoCl_2$ as previously performed for PTKs.[20]

4.4 Preliminary Results

Thermoplastic poly(thioketal urethane) (TPTKUR) thermal analysis. TPTKUR elastomers were synthesized both with and without butane diol (BDO) chain extenders (**Figure 4.1A**). TPTKURs will be referred to as (hard segment)-(*optional chain extender)*-(soft segment) throughout the paper (e.g. HDI-BDO-MEE). DSC scans were run on all synthesized TPTKURs to determine both T_g and T_m. Glass transition temperature is a physical characteristic of the TK macrodiols and pure TK macrodiols T_g is reported near -75 ºC. Phase-separated TPURs express independent T_g near that of pure soft segment T_g, while phase-mixed T_g occurs well above that of pure soft segment T_g. For all six TPTKURs investigated, DSC revealed T_g transitions occurring between -60 ºC and -36 ºC (**Figure 4.1B**). DSC also showed T_m for all synthesized TPTKUR, DSC runs were limited to 200 ºC, as any polymer above this temperature would be unsuitable for FDM applications. The T_m for both the HDI-BDO-MEE and CHDI-EDDT was promising near 180 ºC, while HDI-BDO-EDDT showed a low T_m near 50 ºC (**Figure 4.1C**). For the remaining three TPTKURs, the melting temperature was not present in the DSC run and assumed to be > 200 ºC and undesirable for our applications. TGA on a representative elastomer (CHDI-MEE) showed polymer thermal instability and degradation occurring at 250 ºC, as percent mass decreased rapidly at this temperature (**Figure 4.1E**). *In vitro* oxidative degradation was tested on a representative TPTKUR elastomer (CHDI-BDO-MEE) by tracking percent mass loss in ROS media. After one day in oxidative media, the elastomer lost more than 50% of its original mass and by day 5 had completely degraded.

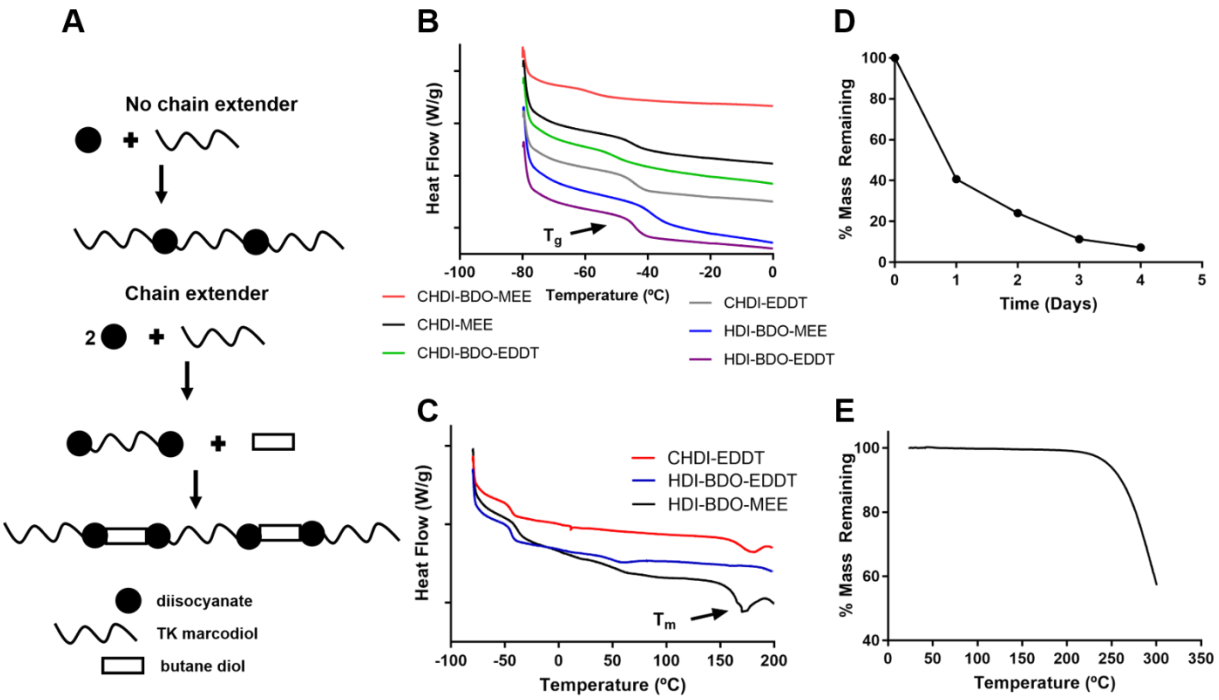

Figure 4.1: Synthesis and characterization of TPTKUR elastomers. (A) TPTKUR synthesis pathway with and without chain extenders. (B-C) DSC scans showing (B) T_g and (C) T_m. (D) CHDI-BDO-MEE degradation in 20% H_2O_2 /0.1 M $CoCl_2$ solution showing mass loss over time. (E) TGA scan showing CHDI-MEE thermal instability at 250 ºC.

Morphological Analysis of TPTKURs by FTIR. The extent of microphase-separation was assessed by FTIR on all six thermoplastic elastomers. Carbonyl bonds (C=O) within hard segment urethane linkages can be visualized as sharp peaks at 1720 cm^{-1} and amine bonds (N-H) as a broad peak around 3300 cm^{-1}. Hydrogen bonding can shift these peaks slightly and the extent of shifting can be attributed to the extent of microphase-separation occurring in the thermoplastic elastomers. Yilgor et al. have reported free (non-H-bonded) carbonyl peaks for similar TPURs occurring at 1732 cm^{-1} and strong hydrogen bonded (H-bonded) carbonyl peaks occurring at 1685 cm^{-1}.[22] Representative elastomers HDI-BDO-MEE and CHDI-BDO-MEE reveal peaks occurring at the same positions reported by Yilgor with H-bonded C=O peaks appearing larger than non-H-bonded peaks for both elastomers (**Figure 4.2A-B**). The extent of microphase-separation was quantified

for all elastomers by peak integration of H-bonded and non-H-bonded area and reported as %H-bonded C=O by total area. (**Table 4.1**). All six elastomers evaluated revealed H-bonded peaks, with the greatest phase-separation reported as HDI-BDO-MEE at 62% and the least %H-bonding as CHDI-MEE at 37%. Amine H-bonding was also assessed on representative elastomers (HDI-BDO-MEE). Yilgor et al., reports as a similar TPURs cools, microphase-separation can be assessed by the shift of amine peaks (N-H) from a weak, broad peak at 3336 cm^{-1} to a stronger, sharper peak at 3321 cm^{-1}.[22] When HDI-BDO-MEE cooling was assessed by FTIR, similar peak shifts were visualized over at 30 minute time course study (**Figure 4.2C-D**).

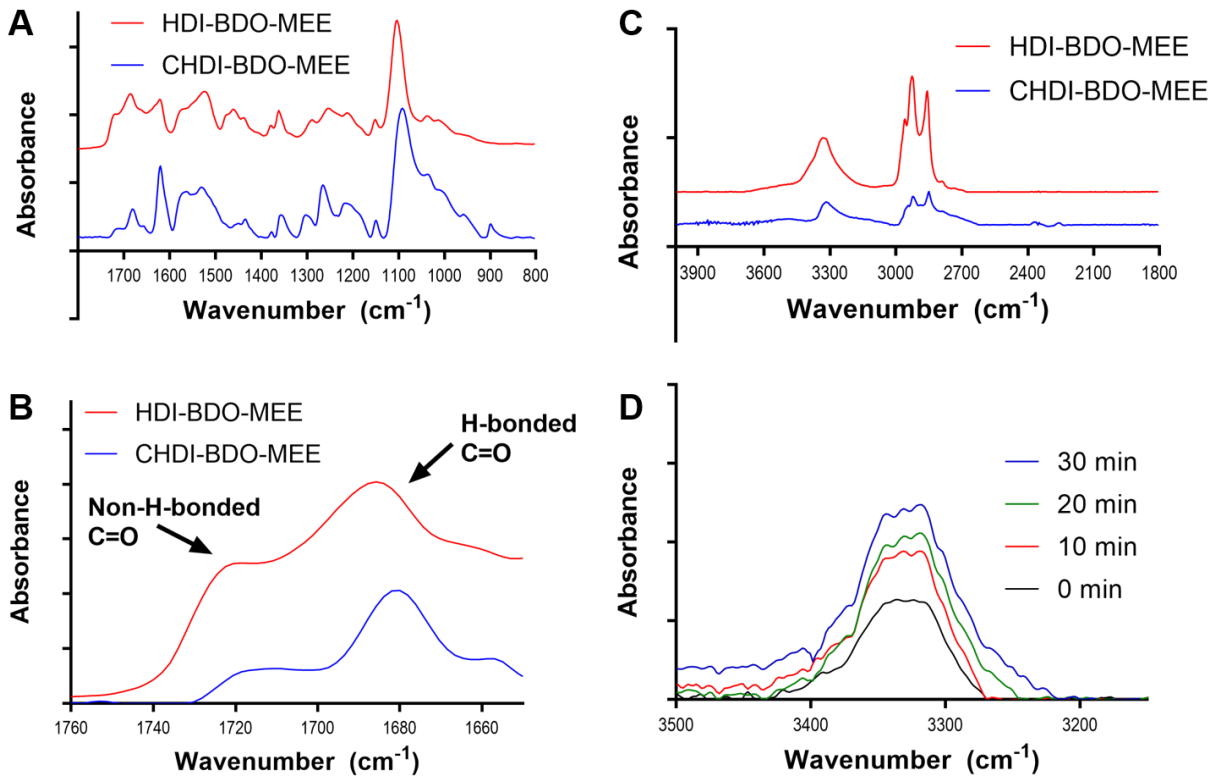

Figure 4.2: Morphological analysis of TPTKUR elastomers by FTIR. Spectra of HDI-BDO-MEE and CHDI-BDO-MEE showing (A-B) hydrogen-bonded and non-hydrogen-bonded C=O groups and (C-D) sharpening of the N–H peak over time due to hydrogen bonding with C=O groups. (D) HDI-BDO-MEE peak sharpening time course.

ISO	Chain Ex	TK	HS wt%	T_g °C	T_m °C	%H-bonded C=O area
CHDI	BDO	MEE	29.7	-60	>200	59
HDI	BDO	MEE	29.9	-36	165	62
CHDI	BDO	EDDT	25.3	-50	>200	50
HDI	BDO	EDDT	25.4	-44	56	53
CHDI	-	MEE	14.2	-45	>200	37
CHDI	-	EDDT	11.7	-47	179	50

Table 4.1: TPTKURs summary table. Isocyanate, chain extender and thioketal (TK) content in each sample. Hard segment weight percent calculations are reported along with all thermal and morphological experimental findings.

4.5 Discussion

In this preliminary study, thermoplastic poly(thioketal urethanes) (TPTKUR) were synthesize and characterized using a new oxidatively degradable family of thioketal (TK) soft segment macrodiols. Selection of precursors and synthesis methods were driven largely by prior studies and reported findings.[6, 8, 10, 16, 23] Symmetric diisocyanate hard segments, with or without chain extender, were selected as the Wilkes group had found microphase- separation and the creation of ideal elastomeric polymers were driven by symmetry. They show symmetry creates a highly percolated bands of hard segments visualized by atomic force microscopy (AFM) and report spacing between hard segments bands by small angle X-ray scattering (SAXS) and wide angle X-ray scattering (WAXS).[24] Yilgor et al. furthered these findings by revealing H-bonding within hard segments is a driving force for microphase-separation, and that symmetric hard segments allow for greater H-bonding over an asymmetric diisocyanate.[22]

Initially, MEE and EDDT-based PTK macrodiols were selected for screening TPTKUR elastomers as the molecular weight (1100 – 1250 g/mol) and calculated solubility parameters were similar to reported soft segments in similar studies.[13] A previous study showed favorable results

in vivo using the MEE-based PTK macrodiol, so this formulation was chosen moving forward in this study.[6] It was hypothesized that maximizing PTK content within the elastomers would lead to a more favorable, and a less toxic biomaterial. The hard segment diisocyanate is not known to be highly biocompatible, so minimizing the hard segment weight percent was a design criterion under consideration. Maximizing PTK content would also lead to greater degradability of the thioketals and ethers present in the PTK structure.[6] Chain extenders have historically been used to create stable TPURs, but the additions of BDO chain extenders increases the hard segment weight percent in our TPTKUR (25.3% – 29.9%) elastomers (**Table 4.1**). Recently, studies have reported the creation of TPUR elastomers without chain extenders which posess favorable thermal properties and are highly microphase-separated.[16, 17, 25] By creating TPTKURs without chain extenders, we can greatly reduce hard segment content in our elastomers (11.7% - 14.2%) and maximize soft segment TK macrodiol weight percent (**Table 4.1**).

Preliminary results show microphase-separation, to a certain extent, was achieved in all six TPTKURs synthesized. The T_g values for all elastomers were in acceptable ranges of below -36 ºC which is comparable to the thermal properties of pure TK macrodiol. This suggests the elastomer is thoroughly microphase-separated, as soft segment content is not phase mixing with the hard segment content, and thermodynamic incompatibilities of the two phases have been achieved. Yet, the melting temperatures for all materials are not in the desirable range for future extrusion and FDM printing. Ideally, we are seeking a material with a T_m in the range above body temperature, but below the temperature at which the elastomer begins to breakdown. Two promising candidates emerged from these preliminary results, HDI-BDO-MEE and CHDI-EDDT as the melting temperatures were near 170 ºC. TGA data showed any T_m above 200 ºC could lead to polymer degradation during extrusion, so polymers with T_m above this temperature would not

be acceptable for use moving forward. While CHDI-EDDT revealed promising thermal properties, the CHDI hard segment precursor was challenging in practice to react with TK macrodiol soft segments. GPC showed low molecular weight of the final polymer suggesting low conversion of CHDI at reaction conditions. This may be due to the high melting temperature of CHDI as a precursor (62 ºC) and difficulty dissolving CHDI in DMF reaction solvent. The T_m of CHDI-EDDT elastomer may be due to low conversion and low molecular weight rather than ideal elastomeric thermal properties. HDI-BDO-MEE did emerge as a promising candidate as its physical and thermal properties were within the acceptable ranges. FITR affirmed these conclusions as HDI-BDO-MEE showed the greatest %H-bonding carbonyl bonds. The anime peaks also showed similar peak shifting and sharpening associated with favorable microphase-separation.[22]

4.6 Conclusion and Future Directions

This work presents the creation of a favorably microphase-separated thermoplastic poly(thioketal urethane) (TPTKUR) elastomer capable of degradation by cell-mediated release of reaction oxygen species during cellular infiltration. DSC and FTIR testing confirm desired thermal and morphological properties of the TPTKUR elastomers have been achieved and helped to select a promising TPTKUR formulation (HDI-BDO-MEE) for further testing.

DSC is a powerful tool for evaluating thermal properties, but to determine bulk material properties, dynamic mechanical analysis (DMA) testing will need to be performed to further assess thermal transition such as T_g and T_m of polymer films. And while FTIR is an effective way to assess morphological details of elastomers, microphase-separation can be further tested by SAXS and WAXS to characterize repeating percolated hard segment nanostructures and determine spacing between these segments. To visualize and qualitatively assess microphase-separation of

the elastomers, AFM testing should be performed to further prove the desired nanostructure has been achieved. Once polymer characterization has been completed and ideal thermal and mechanical properties have been determined, polymer films should be extruded into filaments for use in FDM printers. These polymers may then be printed into desired tissue scaffolding for *in vitro* and *in vivo* testing moving forward.

4.7 References

1. Chia, H. N.; Wu, B. M., Recent advances in 3D printing of biomaterials. *Journal of Biological Engineering* **2015,** *9* (1), 4.
2. Xu, N.; Ye, X.; Wei, D.; Zhong, J.; Chen, Y.; Xu, G.; He, D., 3D artificial bones for bone repair prepared by computed tomography-guided fused deposition modeling for bone repair. *ACS Appl Mater Interfaces* **2014,** *6* (17), 14952-63.
3. Buyuksungur, S.; Endogan Tanir, T.; Buyuksungur, A.; Bektas, E. I.; Torun Kose, G.; Yucel, D.; Beyzadeoglu, T.; Cetinkaya, E.; Yenigun, C.; Tonuk, E.; Hasirci, V.; Hasirci, N., 3D printed poly(epsilon-caprolactone) scaffolds modified with hydroxyapatite and poly(propylene fumarate) and their effects on the healing of rabbit femur defects. *Biomater Sci* **2017,** *5* (10), 2144-2158.
4. Vanderburgh, J.; Sterling, J. A.; Guelcher, S. A., 3D Printing of Tissue Engineered Constructs for In Vitro Modeling of Disease Progression and Drug Screening. *Ann Biomed Eng* **2017,** *45* (1), 164-179.
5. Feuerbach, T.; Callau-Mendoza, S.; Thommes, M., Development of filaments for fused deposition modeling 3D printing with medical grade poly(lactic-co-glycolic acid) copolymers. *Pharm Dev Technol* **2018**, 1-7.
6. Martin, J. R.; Gupta, M. K.; Page, J. M.; Yu, F.; Davidson, J. M.; Guelcher, S. A.; Duvall, C. L., A porous tissue engineering scaffold selectively degraded by cell-generated reactive oxygen species. *Biomaterials* **2014,** *35* (12), 3766-76.
7. McEnery, M. A.; Lu, S.; Gupta, M. K.; Zienkiewicz, K. J.; Wenke, J. C.; Kalpakci, K. N.; Shimko, D. A.; Duvall, C. L.; Guelcher, S. A., Oxidatively degradable poly (thioketal urethane)/ceramic composite bone cements with bone-like strength. *RSC advances* **2016,** *6* (111), 109414-109424.
8. Spaans, C. J.; De Groot, J. H.; Belgraver, V. W.; Pennings, A. J., A new biomedical polyurethane with a high modulus based on 1,4-butanediisocyanate and e-caprolactone. *Journal of Materials Science: Materials in Medicine* **1998,** *9*, 675-678.
9. Spaans, C. J.; De Groot, J. H.; Van der Molen, L. M.; Pennings, A. J., New biodegradable polyurethane-ureas, polyurethane and polyurethane-amide for in-vivo tissue engineering: structure-properties relationships. *Polymeric Materials Science and Engineering* **2001,** *85*, 61-62.
10. Yilgor, I.; Yilgor, E.; Wilkes, G., Critical parameters in designing segmented polyurethanes and their effect on morphology and properties: A comprehensive review. *Polymer* **2015,** *58*, A1-36.
11. Sami, S.; Yildirim, E.; Yurtsever, M.; Yurtsever, E.; Yilgor, E.; Yilgor, I.; Wilkes, G., Understanding the influence of hydrogen bonding and diisocyanate symmetry on the morphology and properties of segmented polyurethanes and polyureas: computational and experimental study. *Polymer* **2014,** *55* (18), 4563-76.
12. Sheth, J.; Klinedinst, D.; Wilkes, G.; Iskender, Y.; Yilgor, I., Role of chain symmetry and hydrogen bonding in segmented copolymers with monodisperse hard segments. *Polymer* **2005,** *46* (18), 7317-22.
13. Sonnenschein, M. F., *Polyurethanes : Science, Technology, Markets, and Trends*. 1 ed.; John Wiley & Sons, Inc.: Online, 2014.
14. Leibler, L., Theory of microphase separation in block co-polymers *Macromolecules* **1980,** *13* (6), 1602-17.

15. Klinedinst, D.; Yilgor, E.; Yilgor, I.; Beyer, F.; Wilkes, G., Structure-property behavior of segmented polyurethaneurea copolymers based on an ethylenebutylene soft segment. . *Polymer* **2005,** *46* (23), 10191-201.
16. Klinedinst, D. B.; Sheth, J. P.; Yilgor, E.; Yilgor, I.; Beyer, F. L.; Wilkes, G. L., Structure - property behavior of new segmented polyurethanes and polyureas without use of chain extenders. *Rubber Chemistry and Technology* **2005,** *78*, 737-753.
17. Das, S.; Cox, D.; Wilkes, G.; Klinedinst, D.; Yilgor, I.; Yilgor, E., Effect of symmetry and H-bond strength of hard segments on the structure-property relationships of segmented, nonchain extended polyurethanes and polyureas. *J Macromol Sci Part B Phys* **2007,** *46* (5), 853-75.
18. Marcus, Y., Solubility Parameters of Permanent Gases. *Journal of Chemistry* **2016,** *2016*, 4701919.
19. Guo, R.; Ward, C. L.; Davidson, J. M.; Duvall, C. L.; Wenke, J. C.; Guelcher, S. A., A transient cell-shielding method for viable MSC delivery within hydrophobic scaffolds polymerized in situ. *Biomaterials* **2015,** *54*, 21-33.
20. Martin, J. R.; Gupta, M. K.; Page, J. M.; Yu, F.; Davidson, J. M.; Guelcher, S. A.; Duvall, C. L., A porous tissue engineering scaffold selectively degraded by cell-generated reactive oxygen species. *Biomaterials* **2014,** *35* (12), 3766-3776.
21. Yilgor, E.; Yilgor, I.; Yurtsever, E., Hydrogen bonding and polyurethane morphology. I. Quantum mechanical calculations of hydrogen bond energies and vibrational spectroscopy of model compounds. *Polymer* **2002,** *43* (24), 6551-9.
22. Yilgor, I.; Yilgor, E.; Guler, G.; Ward, T. C.; Wilkes, G. L., FTIR investigation of the influence of diisocyanate symmetry on the morphology development in model segmented polyurethanes. *Polymer* **2006,** *47*, 4105-4114.
23. Yilgor, I.; Eynur, T.; Bilgin, S.; Yilgor, E.; Wilkes, G., Influence of soft segment molecular weight on the mechanical hysteresis and set behavior of silicone-urea copolymers with low hard segment contents. . *Polymer* **2011,** *52* (2), 266-74.
24. Klinedinst, D. B.; Yilgör, I.; Yilgör, E.; Zhang, M.; Wilkes, G. L., The effect of varying soft and hard segment length on the structuree property relationships of segmented polyurethanes based on a linear symmetric diisocyanate, 1,4-butanediol and PTMO soft segments. *Polymer* **2012,** *53*, 5358-5366.
25. Das, S.; Yilgor, I.; Yilgor, E.; Inci , B.; Tezgel, O.; Beyer, F.; Wilkes, G., Structure-property relationships and melt rheology of segmented, non-chain extended polyureas: Effect of soft segment molecular weight. *Polymer* **2007,** *48*, 290-301.

APPENDIX

Appendix A: nHA-LTI Grafting Model Development

$$NCO + OH - nHA \rightarrow urethane - nHA$$

$$rate = \frac{-d[NCO]}{dt} = k[NCO][OH]$$

[NCO] and [OH] are concentrations of reactive NCO groups and nHA surface OH groups. k is the reaction constant.

Since urethane reaction involves one NCO group and one OH group, the amount of consumed NCO groups is equal to the amount of consumed OH groups.

$$[OH]_0 - [OH] = [NCO]_0 - [NCO]$$

$[OH]_0$ and $[NCO]_0$ are initial concentrations of OH groups and NCO groups at $t=t_0$, respectively. They can be calculated based on formulation and known equivalency of NCO and OH present on LTI and nHA respectively.

Let $C_0 = [OH]_0 - [NCO]_0$

$$[OH] = [OH]_0 - [NCO]_0 + [NCO] = C_0 + [NCO]$$

$$rate = \frac{-d[NCO]}{dt} = k[NCO][OH] = k[NCO](C_0 + [NCO])$$

$$kdt = \frac{-d[NCO]}{[NCO]([NCO] + C_0)} = \frac{-d[NCO]}{C_0}\left(\frac{1}{[NCO]} - \frac{1}{C_0 + [NCO]}\right)$$

$$C_0 k \int_{t_0}^{t} dt = \int_{[NCO]_0}^{[NCO]} \frac{1}{C_0 + [NCO]} d[NCO] - \int_{[NCO]_0}^{[NCO]} \frac{1}{[NCO]} d[NCO]$$

$$C_0 k(t - t_0) = ln(C_0 + [NCO]) - ln(C_0 + [NCO]_0) - ln[NCO] + ln[NCO]_0$$

Note $C_0 + [NCO]_0 = [OH]_0$ *and* $t_0 = 0$, thus

$$C_0 kt = ln(C_0 + [NCO]) - ln[OH]_0 - ln[NCO] + ln[NCO]_0$$

$$\boxed{C_0 kt + ln\left(\frac{[OH]_0}{[NCO]_0}\right) = ln\left(\frac{C_0 + [NCO]}{[NCO]}\right)}$$

Appendix B: Laboratory Standard Operating Procedures

Principle:

Grafting lysine triisocyanate (LTI) onto nanohydroxyapatite (nHA) under dry conditions.

Before starting:

- Dry glassware in oven overnight and allow to cool before use.
- Personal protective and safety equipment required:
    - Disposable nitrile gloves
    - Hood
    - Appropriate attire according to the Chemical Hygiene Plan (shoes, labcoat, goggles, etc.)

Procedure:

1. Place nHA in vacuum oven at 80 ºC for at least 48 hours.
2. Add desired amount of nHA to three neck RBF with stir bar.
3. Attach rubber septa on middle and right neck of RBF and a glass stopcock on left neck.
4. Apply vacuum through glass stopcock. Heat the RBF with heat gun under vacuum for 3-5 minutes.
5. Setup oil bath below RBF and set temperature to 80 ºC, adjusting slowly to avoid overshoot.
6. Place RBF into oil bath and allow nHA to dry under vacuum for at least 24 hours.
7. Reset temperature of oil bath to 40 ºC and allow system to cool.
8. Replace vacuum with N_2 filled balloon and open nitrogen to reaction.
    a. Fit balloon to end of short piece of vacuum tubing and rubber band to secure.
    b. Close valve and remove vacuum line.
    c. Fill balloon with N_2 gas and twist at top to hold gas in for transfer.
    d. Fit vacuum line with balloon to glass stopcock, release twisted balloon and open stopcock to reaction.
9. Add lysine triisocyanate (LTI) to RBF using syringe with needle through rubber septa.
10. Allow reaction to stir for at least 16 hours at 40 ºC at stir rate to 250 rpm.
    a. If LTI and nHA are not dispersing well, use a 12” needle to manually mix solution carefully until nHA and LTI evenly disperse.

Principle:

Prepare oxidative degradation media for *in vitro* degradation studies. This media will contain 20 wt% hydrogen peroxide and 0.1M cobalt chloride.

Before starting:

- Read and understand the MSDS of the reagents listed below
- Personal Protective and Safety Equipment required:
    - Disposable nitrile gloves
    - Heavy duty gloves
    - Hood
    - Appropriate attire according to the Chemical Hygiene Plan (shoes, labcoat, goggles, etc.)

Reagents:

- 30 wt% hydrogen peroxide (Sigma Aldrich)
- Cobalt chloride hexahydrate (Fisher)
- Water

Materials and Equipment:

- 1 beaker (size depends on batch size)
- Glass bottle
- Foil
- Stir plate
- Stir bar

Procedure (All listed values are for a 1L batch size)

1. Make sure all glassware is washed and dried prior to use
2. Dissolve cobalt chloride in water (23.78 g COCl2 hexahydrate in 333 mL water) in a glass beaker
3. In the glass bottle, measure out required amount of 30 wt% hydrogen peroxide (667 mL)
4. Add COCl2 solution to hydrogen peroxide slowly while stirring
5. Cover glass bottle with foil and store in the refrigerator

Notes:

- Addition of COCl2 to H2O2 can produce heat and gas. Make this solution in the hood.
- COCL2(s) will react vigorously with H2O2, so make sure COCl2 is fully dissolved

Clean-up:

1. Collect all glass waste (pipettes, vials, or broken glass) and dispose in the broken glass container (box)
2. Collect all sharps and dispose in the sharps waste container (red box)
3. Oxidative media waste contains heavy metals and must be collected and disposed of properly
4. Clean glassware:
    a. Wash with soap and water
    b. Rinse with acetone and dry in the oven

5% FeAA in ε-caprolactone

Reagents:

- ε-caprolactone (Acros Organics 173442500)
- Magnesium sulfate (Sigma M7506)
- Iron (iii) acetylacetonate (FeAA) (Acros Organics 119130250 or Sigma S17003)

Materials:

- 100 mL beaker
- Magnetic stir bar
- Funnel filter paper
- Glass funnel
- 20 mL vial
- Small magnetic stir bar for vial

Procedure:

1. Dry ε-caprolactone.
    a. Weigh desired amount of ε-caprolactone into beaker with stir bar. (Does not need to be exact weight at this point. Account for loss in filtering step.)
    b. Weigh out and add magnesium sulfate (1g for 10g of ε-caprolactone, doesn't have to be exact) and add to beaker.
    c. Cover with parafilm and allow to stir for 30 minutes on stir plate.
    d. Filter dry ε-caprolactone
        i. Tare a new, clean 20 mL vial
        ii. Place filter paper in glass funnel and pour ε-caprolactone and magnesium sulfate mixture through filter paper into vial. (May take a while for all ε-caprolactone to drip out. Try to cover/seal with parafilm so moisture isn't allowed back in.)
2. Add necessary amount of FeAA to ε-caprolactone for 5% FeAA in ε-caprolactone.

(ie. 10 g ε-caprolactone : 0.5263 g FeAA)

3. Add stir bar and allow to stir until FeAA is dissolved and particles are no longer evident.

Clean-up

5. Dispose of any solid waste into appropriate container.
6. Place glassware into KOH/propanol base bath.
7. Rinse with plenty of cold running water.
8. Rinse with acetone and dry in oven.

Hydroxyl Functionalized Thioketal Crosslinker – Scale up

Protocol is specific to a 30 g batch size. Scale reagents according to runsheet for desired batch size.

Reaction Scheme:

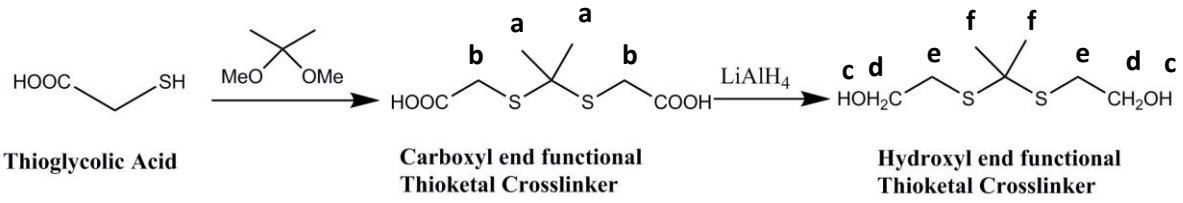

Thioglycolic Acid **Carboxyl end functional Thioketal Crosslinker** **Hydroxyl end functional Thioketal Crosslinker**

Before starting:

- Read and understand the MSDS of the reagents listed below.
- Dry glassware in oven overnight and allow to cool before use.
- Personal protective and safety equipment required:
  - Disposable nitrile gloves
  - Hood
  - Cleanroom face mask – Fisherbrand 18-960B
  - Appropriate attire according to the Chemical Hygiene Plan (shoes, labcoat, goggles, etc.)

Reagents: (store at RT unless otherwise noted)

- Acetonitrile (anhydrous) – Sigma 271004 (1 L Sure/Seal™ containers)
- Bismuth(III) chloride ($BiCl_3$) – Sigma 224839
- 2,2-dimethoxypropane (DMP) – Sigma D136808
- Thioglycolic acid (TGA): **Fatal if inhaled, wear mask when using** – Sigma T3758, store at -20° C
- Lithium Aluminum Hydride ($LiAlH_4$): **Releases flammable gases when in contact with water** – Sigma 199877
- Tetrahydrofuran (THF) (anhydrous, contains 250 ppm BHT as inhibitor) – Sigma 186562 (100 mL Sure/Seal™ containers)
- Diethyl ether (anhydrous) – Sigma 296082
- Sodium hydroxide (1M in water) – Sigma 221465
- Sodium sulfate – Sigma 239313
- Acetone

Materials and Equipment:

- 1 L three neck round bottom flask (RBF)
- 2 L three neck RBF
- 1 L RBF
- Egg shaped stir bar
- Glass stopcock (one-way, flow control adapter)
- Glass stopper
- Rubber septa
- Mechanical stirrer
- Stir rod and accessories

- 24 mL syringe(x2)
- 60 mL syringe
- 16-20 gauge needles (x3)
- 18-20 gauge, 12 in. needle (Sigma 20G - Z261300)
- 16-20 gauge cannula (Sigma 20G - Z101095)
- Balloon & short vacuum tubing (x2)
- Glass hose connector/adapter
- Reflux condenser
- Addition funnel
- Erlenmeyer Flask
- Buchner flask (x2)
- Buchner funnel (x2)
- Filter paper – Whatman 1820-070 Glass Microfiber binder free filter
- Separation funnel (2L)

Procedure for 30 g Batch Size:

Carboxylic End Functional Thioketal Crosslinker Synthesis

1. Add $BiCl_3$ (2.15 g, 6.51 mmol, 0.01X + slight excess) to 1 L three neck RBF with football stir bar.
2. Attach septum in middle neck, one-way glass stopcock on left and a rubber septa on the right neck. Grease and clip glass connections.
3. Apply vacuum through glass stopcock. Heat the RBF with heat gun under vacuum for 3-5 minutes to ensure completely dry catalyst conditions. Allow to cool to RT under vacuum.
4. Replace vacuum with N_2 filled balloon and open nitrogen to reaction.
    a. Fit balloon to end of short piece of vacuum tubing and rubber band to secure.
    b. Close valve and remove vacuum line.
    c. Fill balloon with N_2 gas and twist at top to hold gas in for transfer.
    d. Fit vacuum line with balloon to glass stopcock, release twisted balloon and open stopcock to reaction.
5. Add 500 mL anhydrous acetonitrile to RBF using N_2 to push solvent through cannula into reaction vessel to dissolve $BiCl_3$. Allow $BiCl_3$ to dissolve before moving to next step.
    a. Insert tip of cannula into Sure/Seal ™ cap, keep above liquid.
    b. Insert needle with low N_2 flow into Sure/Seal™ cap.
    c. Insert other end of cannula through rubber stopper into reaction vessel.
    d. Push cannula into acetonitrile to begin transfer.
    e. When about ½ of 1 L bottle has been transferred, remove cannula from reaction first to maintain inert reaction conditions.
6. Add 2,2-dimethoxypropane (95.77 mL, 781.59 mmol -1.2X) to RBF using syringe with needle through rubber septa. (Can use 12” needle if difficult to reach reagent in bottle)
7. Add thioglycolic acid (46 mL, 651.32 mmol – 1X) to RBF using syringe with needle through rubber septa. (Can use 12” needle if difficult to reach reagent in bottle)
8. Allow reaction to stir for 24 hours at RT, 250 rpm.

9. Filter product using a Buchner funnel.
10. Record mass of oven-dried 1 L RBF with stopper.
11. Pour product into tared RBF and rotovap acetonitrile off with water bath at 30-35°C.
12. Attach glass hose connector/adapter and dry under high vacuum for at least 24 hours (2-3 days desirable) to yield completely dry carboxylic acid functional thioketal crosslinker as a dark red, solid (probably stuck to RBF walls). Store in refrigerator if not immediately performing hydroxyl functionalization.
13. NMR in DMSO to verify structure.
    a. δ 1.59, s (**a**)
    b. δ 3.32, s (**b**)

Clean-up: Thiol reaction creates very strong odor that will be on all glassware and anything that comes into contact with TGA or product.

9. Dispose of any solid waste in a waste bag to be left in hood until disposal (including gloves that may have come into contact with TGA or product).
10. Dispose of sharps in sharps waste container.
11. Clean long needles:
    a. Attach to new, clean 3 mL syringe
    b. Pour acetone into beaker
    c. Pull acetone through syringe and expel multiple times
    d. Wipe down exterior with acetone and chemwipes
    e. Dry in oven
12. Clean glassware:
    a. Rinse glassware with acetone or DCM into waste container.
    b. Leave glassware in hood overnight if possible. If not, continue directly to step c.
    c. Introduce glassware into the base bath for 24 hrs. Rinse with a lot of cold running water after removing from the base bath.
    d. Rinse with acetone and dry in the oven.

Hydroxyl Functionalization

1. Clear any unrelated reagents from hood and bring scale into hood.
2. Set condenser to 10-15 °C and set up 2 L three neck RBF with mechanical stirrer in the center, reflux condenser in left neck (side closest to vacuum pump, capped with one way glass stopcock), and addition funnel (capped with rubber septum) in right neck. Apply vacuum grease and clip glass connections.
3. Apply vacuum through condenser and use hot air gun on RBF for 3-5 minutes to ensure glassware assembly is thoroughly dried. Cool completely under vacuum.
4. Replace vacuum line on septum with N_2 filled balloon (follow procedure described above).
5. Find mass of COOH TK by weighing the capped RBF containing the product from above. Subtract mass of RBF and stopper and record mass of COOH TK.
6. Add ~400 mL anhydrous THF to RBF containing COOH TK using nitrogen to push solvent through cannula inserted into RBF (see step 4 above) or a large syringe. Shake/swirl to dissolve TK in solvent.
7. Use mass of COOH TK and run sheet to determine amount $LiAlH_4$ needed.
8. Weigh $LiAlH_4$ (2x mol COOH intermediate) **in fume hood**, close off N_2 balloon and add $LiAlH_4$ to RBF (remove addition funnel in right neck to add $LiAlH_4$, then replace).
    a. Mass closed 25 g container of $LiAlH_4$.
    b. Empty bottle into reactor and re-mass for mass $LiAlH_4$.
    c. Weigh extra needed from open bottle of $LiAlH_4$ using conventional methods.
    d. Re-attach dropping funnel and re-open N_2 valve.
    e. Dispose of anything with contact to $LiAlH_4$ in ziplock bag and place in solid waste bag in hood.
9. Place reaction set up in ice bath.
10. Using large syringe with long needle, add ~350 mL diethyl ether to RBF with $LiAlH_4$.
11. Use cannula and nitrogen or large syringe to transfer TK solution to addition funnel (see step 4 above, may have to fill dropping funnel multiple times until all of TK solution is in reactor).
12. Drop TK solution to stirring RBF at 0°C until all has been added, continually replenishing the ice bath. (3.5-4 hrs.)
    Be very careful, at 0 °C also you will see reflux, so don't add TK solution rapidly (may result in blast or flame from hydrogen generation inside flask).
13. Replace water bath with oil bath. Start stirring slowly (will stir faster once oil is heated) and steadily heat reaction to 52°C to reflux overnight (at least 12 hours). Reflux rate should be about 1 drop/45 seconds at this temperature. Note: Increase heat slowly as it is easy to overshoot oil bath temperature.
    **Ensure reaction is stirring smoothly after a couple of hours in heat with no large solids on top*
14. Cool reaction to room temperature.
15. **Quench $LiAlH_4$ from reaction** **CAUTION!!**
    a. Remove N_2 and stopcock from condenser, but leave condenser attached.
    b. Add about 100 mL of wet ether to dropping funnel (can remove rubber septum at this point).
    c. While stirring, slowly drop in wet ether allowing reaction to cease before dropping more.

   d. Add about 75 mL water to dropping funnel and slowly add to reactor. Add more water if quenching is still evident.
16. Add ~300 mL 1M NaOH through dropping funnel (can have stopcock completely open) while stirring and wait for reaction to subside and product to separate slightly.
17. Using a Buchner funnel and flask, filter out solid by-product.
18. Extract product.
    a. Pour filtered liquid into separation funnel. Shake vigorously releasing pressure 2-3 times and allow to separate until distinct layers are evident. Remove bottom layer (should see a red/brown tinted water layer on the bottom).
    b. Add 75-100 mL of water to separation funnel to wash product. Shake vigorously releasing pressure 2-3 times and allow to separate until distinct layers are evident. Remove bottom layer (should see a red/brown – colorless clear water layer on the bottom) and capture translucent yellow organic layer in an Erlenmeyer flask.
    c. If separation isn't evident, try:
        1. Add diethyl ether solvent.
        2. Add small amount of NaCl salt to separate rag layer.
        3. Add more water and/or NaOH to adjust pH of aqueous layer.
19. Add sodium sulfate to organic solution until sodium sulfate no longer clumps. Leave covered in refrigerator an hour-overnight for complete water removal.
20. Filter out sodium sulfate through Buchner funnel.
21. Tare 1 L RBF, then slowly pour solution into RBF for rotovap (use ether to rinse flask into RBF).
22. Rotovap solvent off with water bath not exceeding 40 °C.
23. Attach glass hose connector/adapter and dry under high vacuum at least 48 hours to remove organic solvents trapped in compound to yield OH functionalized TK crosslinker as a yellow/orange viscous liquid.
24. Can continue to add diethyl ether to solids from step 11 to salvage more TK from reaction. Repeat steps 11-17 if it appears compound is being removed (indicated by yellow color-change of solvent). Keep separate in case impure.
25. NMR in DMSO to verify structure.
    a. δ 4.84, s (**c**) - 2
    b. δ 3.33, t (**d**) - 4
    c. δ 2.56, t (**e**) - 4
    d. δ 1.59, s (**f**) - 6

Clean-up: Thiol reaction creates very strong odor that will be on all glassware and anything that comes into contact with TGA or product.

1. Dispose of any solid waste in a waste bag to be left in hood until disposal (including gloves that may have come into contact with TGA or product).
2. Dispose of sharps in sharps waste container in hood.
3. Clean glassware:
    a. Rinse glassware from making acid solution in sink, flushing with a lot of water to dilute.
    b. Rinse glassware in hood with water bottle into waste container labeled for reaction.
    c. Rinse again with acetone or DCM into waste container.

d. Leave glassware in hood overnight if possible. If not, continue directly to step d.
e. Introduce glassware into the base bath for 24 hrs. Rinse with a lot of cold running water after removing from the base bath.
f. Rinse with acetone and dry in the oven.

Guelcher Lab
µCT Analysis of Cylindrical Defects

Principle:

Rotate 2D reconstruction and analyze bone parameters for cylindrical defects of various lengths and diameters using the µCT50.

Rotation Procedure

Goal: Rotate 2D reconstruction so that a circle normal to the insertion of the defect is visible in the XY plane. See **Figure 1** for desired defect orientation as viewed in each plane.

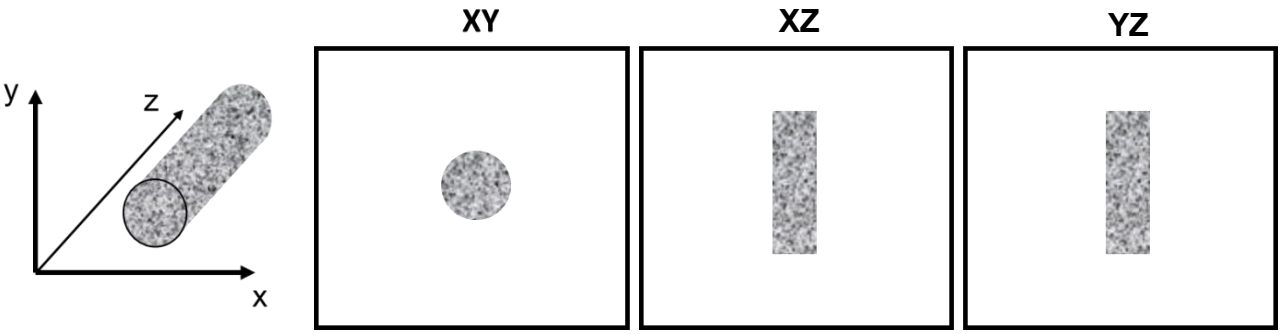

Figure 1. Desired defect orientation for analysis.

1. Load ISQ file of interest so that defect is visible in XZ and YZ planes. (can load every 5th or 10th slice, ie. click bar of slider so that every 10th slice loads)

2. In XZ plane, use angle tool to measure rotation angle necessary to orient defect according to **Figure 1** in that plane.

3. Repeat in YZ plane.

4. Return to XY plane and contour entire defect using box or circle that ensures all of defect is included. Contour selection through entire scan.

5. Use script 28 to rotate.
    a. Input rotation angles measured in blanks for appropriate axes and run script. The axis of rotation will be the axis **not** included in the name of the plane in which the angle measurement was made (ie. If angle measured in XZ plane, the rotation will be done about the Y axis).
    b. MISC:misc1 = x rotation (cw)
    c. MISC:misc2 = y rotation (ccw)
    d. MISC = z rotation (cw)

6. Open new ISQ file generated from the first rotation ("…R.ISQ") and complete any additional rotations necessary by repeating steps 1-5. *Note: may take over an hour to generate new ISQ file.

Measurement Procedure

Goal: Measure bone parameters of cylindrical defect in 4 radial sections assigned by concentric cylinders according to **Figure 2** using script #231 after completing rotations. Green circle is the diameter of the defect.

1. Determine the size of the large outer circle (blue) to be contoured for analysis.
    a. Determine the value of X in schematic using scan voxel size (voxel = µm/slice).
        Ex: 5 mm defect, 17.2 µm voxel size.
        5 mm = 6X ∴ X = 0.833 mm
        → 17.2 µm/slice ∴ X = 48.4 slices
        Larger circle = 8X ∴ **Larger circle ≈ 387**

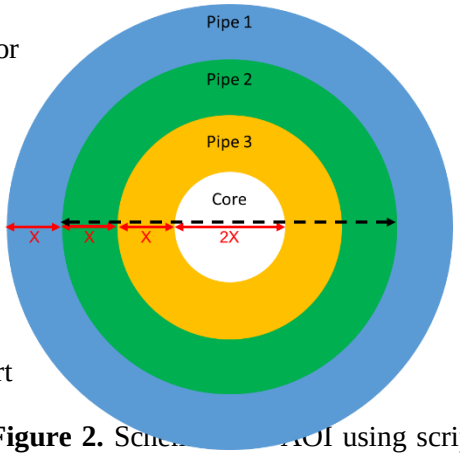

Figure 2. Schematic of ROI using script 231. The green circle (dotted line) is the defect diameter, the blue circle is the circle drawn during contouring. Program outputs bone parameters for colored rings.

2. Determine desired length of measurement. Use voxel size to convert this to number of slices.

3. On the first slice within desired length range, use circle tool to draw circle with the size determined in a. The size readout is in the bottom left box of the µCT screen (ie. WxH: 387 x 387 [p]). Use "ctrl + c" command to copy circle and location.

4. Scroll to final slice of length selection and use "insert" key or "ctrl + v" to paste same circle there.

5. Use contour range to morph the shape throughout the selection.
    *Note: If defect is not straight, the circle can be moved slightly throughout the contour. Do not do this for large inconsistencies.

6. Use script #231 to run measurements.
    a. Ensure "Default VOI" is selected to include all of the contouring.
    b. Choose desired filtering ("Gauss Sigma" and "Gauss Support") and thresholding.

7. Data will output to the "Data" folder on MicroCT FTP under the scan number for the sample. Download the file "…Concentric.txt" to retrieve data.
    *Note: Data for "pipe 1" is the BV/TV (and BV, TV) for the volume of the blue ring, "pipe 2" is the data for the volume of green ring, etc.

Principle:
Use safranin O and Fast green to stain for cartilage in ground, PMMA sections.
Adapted from Josh Johnson (Vanderbilt Center for Bone Biology).

Materials:
- • Fast Green Solution (0.2% Fast Green SF in water) – 250 mL
- • Safranin O Solution (0.1% Safranin O in water) – 250 mL
- • Acetic Acid (1% in water) – 1 L

Procedure:
1. Filter stains through filter paper and funnel into separate histology buckets.
2. Add acid to 4 separate 250 mL histology buckets.
3. Stain in Fast Green. 5 min
4. Rinse in fresh acetic acid. Dip
5. Stain in safranin O. 3 min
6. Rinse in fresh acetic acid. Dip
7. Repeat steps 3-5.
8. Blot dry with Kimwipes

Notes:
1. *2 cycles sufficient for rabbit femoral plug defects (30 – 70 μM ground sections). May repeat steps 3-5 until desired color balance.*
2. *May mount slides with coverslips if desired.*

Stain Colors/Detection:
Cartilage – red (in proportion to proteoglycan content)
Bone – green/blue

Clean-up:
1. Dump acetic acid in sink and rinse bucket thoroughly (≤ 1% acid).
2. If still translucent and no cloudiness, add fast green and safranin O back to original containers. Rinse buckets thoroughly in sink.

Principle:

Use immunohistochemistry to detect blood vessels (CD31/PECAM, endothelial cells) and macrophages (CD68) in ground plastic sections. Adapted from Immunohistochemical Staining_AM protocol from Sterling Lab.

Materials:

- Humidifying staining chamber (Sterling lab)
- 4 staining buckets and 1 staining rack (Sterling lab)
- IMMEDGE hydrophobic pen (Fisher Scientific, cat. NC9545623)

Antibodies/detectors:

- Goat anti-Mouse IgG (H+L) Cross-Absorbed Secondary Antibody, HRP (ThermoFisher, cat. 31432)
- CD31/PECAM-1 Antibody (JC/70A) (Novus Biologicals, LLC, cat. NB600-562-0.1ml)
- Anti-CD68 antibody [KP1] (abcam, cat. Ab955)
- ImmPACT NovaRED (Vector Labs, cat.. SK4805)
- Goat serum (Sterling lab)

Reagents:

- Sodium citrate ()
- Tween 20 (Sigma, P1379)
- 1X PBS
- 50% H2O2 (Fisher, H341)
- Methanol
- Aqua-Mount (Thermo Scientific, 13800)

Before starting:

1. Prepare solutions.
    a. **Citrate buffer:** (10mM sodium citrate): 2.94g sodium citrate in 900 mLH2O
        i. pH to 6 using NaOH/HCl
    b. **TPBS:** 500 μL Tween 20 in 1L 1X PBS
    c. **0.5% H2O2:** 2.5 mL H2O2 in 247.5 mL methanol
    ** For use only if using an HRP labeled secondary antibody
    d. **5% Goat serum:** 0.5 mL goat serum in 9.5 mL PBS

Procedure:

1. Antigen retrieval.
    a. Preheat citrate buffer to 80°C in microwave.
    b. Transfer to histology bin. Soak at RT. 1 x 1 hr

2. PBS wash in histology bins. 3 x 3 m
3. Step for HRP labeled secondary only. If no HRP, skip to step 5.
    a. 0.5% H2O2 wash in histology bins. 1 x 10 m
4. PBS wash in histology bins 3 x 3 m
5. Shake off excess water and dry edges with Kimwipe. Draw barrier around section with hydrophobic pen.
6. Block with serum 1 x 1 hr
    a. Arrange slides in humidifying chamber facing up. Drop 5% goat serum using pipettor or transfer pipettes.
    b. Use transfer pipette or Kimwipe (away from defect) to remove serum.
7. Incubate in primary antibodies. overnight
    a. Dilute primary antibodies in goat serum:
    CD68 – 1:200 (ie 20 µL Ab in 4 mL serum)
    CD31 – 1:100 (ie 40 µL Ab in 4 mL serum)
    b. Use pipettor or transfer pipette to drop antibody solution onto slides (around 0.75 mL/slide).
    c. Use transfer pipette or Kimwipe to remove antibodies.
    ***NOTE: These antibodies cannot be used on the same slide. Must use separate slides for each maker.*
8. Add slides to slide holder and wash in TPBS in histology bins. 3 x 3 m
    a. Use Kimwipe to dry area around defect.
9. Incubate in secondary antibodies. 1 x 1hr
    a. Dilute secondary antibody in goat serum:
    Goat anti-mouse IgG-HRP – 1:500
    b. Use pipettor or transfer pipette to drop secondary antibody solution onto slides.
    NOTE: *Use same secondary antibody for both primary antibodies in this procedure.*
10. Add slides to slide holder and wash in TPBS in histology bins. 3 x 3 m
    Use Kimwipe to dry area around defect.
11. Detect with NovaRed Chromagen Kit 12-15m
    a. Make detection solution according to instructions with kit.
    b. Use transfer pipette to add detector solution to slides. Let stand 12 – 15 minutes until color begins to appear.
    c. **Stop reaction with distilled H2O wash in histology bins.**
12. Optionally, mount slides with Permount Mounting solution and glass coverslips being careful to eliminate bubbles.

Notes:

1. *Times listed may vary depending on the sample and section thickness.*
2. *Tested for these antibodies. May be adapted for other targets.*
3. *May counterstain with hematoxylin (Harris Formula) if desired.*